dPeak: High Resolution Identification of Transcription Factor Binding Sites from PET and SET ChIP-Seq Data

Dongjun Chung[1,#], Dan Park[2], Kevin Myers[2], Jeffrey Grass[3,4], Patricia Kiley[2,4], Robert Landick[3,4,5], Sündüz Keleş[1,6,*]

1 Department of Statistics, University of Wisconsin, Madison, WI, U.S.A.
2 Department of Biomolecular Chemistry, University of Wisconsin, Madison, WI, U.S.A.
3 Department of Biochemistry, University of Wisconsin, Madison, WI, U.S.A.
4 Great Lakes Bioenergy Research Center, University of Wisconsin, Madison, WI, U.S.A.
5 Department of Bacteriology, University of Wisconsin, Madison, WI, U.S.A.
6 Department of Biostatistics and Medical Informatics, University of Wisconsin, Madison, WI, U.S.A.
∗ **E-mail: keles@stat.wisc.edu**
Current address: Department of Biostatistics, Yale University, New Haven, CT, U.S.A.

Abstract

Chromatin immunoprecipitation followed by high throughput sequencing (ChIP-Seq) has been successfully used for genome-wide profiling of transcription factor binding sites, histone modifications, and nucleosome occupancy in many model organisms and humans. Because the compact genomes of prokaryotes harbor many binding sites separated by only few base pairs, applications of ChIP-Seq in this domain have not reached their full potential. Applications in prokaryotic genomes are further hampered by the fact that well studied data analysis methods for ChIP-Seq do not result in a resolution required for deciphering the locations of nearby binding events. We generated single-end tag (SET) and paired-end tag (PET) ChIP-Seq data for σ^{70} factor in *Escherichia coli (E. coli)*. Direct comparison of these datasets revealed that although PET assay enables higher resolution identification of binding events, standard ChIP-Seq analysis methods are not equipped to utilize PET-specific features of the data. To address this problem, we developed dPeak as a high resolution binding site identification (deconvolution) algorithm. dPeak implements a probabilistic model that accurately describes ChIP-Seq data generation process for both the SET and PET assays. For SET data, dPeak outperforms or performs comparably to the state-of-the-art high-resolution ChIP-Seq peak deconvolution algorithms such as PICS, GPS, and GEM. When coupled with PET data, dPeak significantly outperforms SET-based analysis with any of the current state-of-the-art methods. Experimental validations of a subset of dPeak predictions from σ^{70} PET ChIP-Seq data indicate that dPeak can estimate locations of binding events with as high as 2 to 21bp resolution. Applications of dPeak to σ^{70} ChIP-Seq data in *E. coli* under aerobic and anaerobic conditions reveal closely located promoters that are differentially occupied and further illustrate the importance of high resolution analysis of ChIP-Seq data.

Author Summary

Chromatin immunoprecipitation followed by high throughput sequencing (ChIP-Seq) is widely used for studying *in vivo* protein-DNA interactions genome-wide. Current state-of-the-art ChIP-Seq protocols utilize single-end tag (SET) assay which only sequences $5'$ ends of DNA fragments in the library. Although paired-end tag (PET) sequencing is routinely used in other applications of next generation sequencing, it has not been much adapted to ChIP-Seq. We illustrate both experimentally and computationally that PET sequencing significantly improves the resolution of ChIP-Seq experiments and enables ChIP-Seq applications in compact genomes like *Escherichia coli (E. coli)*. To enable efficient identification using PET ChIP-Seq data, we develop dPeak as a high resolution binding site identification algorithm. dPeak implements probabilistic models for both SET and PET data and facilitates efficient analysis of both

data types. Applications of dPeak to deeply sequenced *E. coli* PET and SET ChIP-Seq data establish significantly better resolution of PET compared to SET sequencing.

Introduction

Since its introduction, chromatin immunoprecipitation followed by high throughput sequencing (ChIP-Seq) has revolutionized the study of gene regulation. ChIP-Seq is currently the state-of-the-art method for studying protein-DNA interactions genome-wide and is widely used [1–5]. ChIP-Seq experiments capture millions of *DNA fragments* ($150 \sim 250bp$ in length) that the protein under study interacts with using random fragmentation of DNA and a protein-specific antibody. Then, high throughput sequencing of a small region ($25 \sim 100bp$) at the $5'$ end or both ends of each fragment generates millions of *reads* or *tags*. Sequencing one end and both ends are referred to as *single-end tag (SET)* and *paired-end tag (PET)* technologies, respectively (Fig. 1A). Standard preprocessing of these data involves mapping reads to a reference genome and retaining the uniquely mapping ones [6,7]. In PET data, start and end positions of each DNA fragment can be obtained by connecting positions of paired reads [8]. In contrast, the location of only the $5'$ end of each DNA fragment is known in SET data. The usual practice for SET data is to either extend each read to its $3'$ direction by the average library size which is a parameter set in the experimental procedure [7] or shift the $5'$ end position of each read by an estimate of the library size [9]. Then, genomic regions with large numbers of clustered aligned reads are identified as binding sites using one or more of the many available statistical approaches [6, 7, 9–11] (the first step in Fig. 1C).

Currently, the SET assay dominates all the ChIP-Seq experiments despite the fact that PET has several obvious, albeit less studied, advantages over SET. In PET data, paired reads from both ends of each DNA fragment can reduce the alignment ambiguity, increase precision in assigning the fragment locations, and improve mapping rates. This is especially advantageous for studying regulatory roles of repetitive regions of genomes [12,13]. Although many eukaryotic genomes are rich in repetitive elements, PET technology has not been extensively used with eukaryotic genomes [8,14]. One of the main reasons for this is that ChIP-Seq data is information rich even when the repetitive regions are not profiled [15] and that the PET assay costs $1.5 \sim 2$ times more than the SET assay. Put differently, given a fixed cost, PET sequencing results in a lower sequencing depth compared to SET sequencing.

In contrast to eukaryotic genomes, prokaryotic genomes are highly mappable, e.g., 97.8 % of the *Escherichia coli* (*E. coli*) genome is mappable with $32bp$ reads. This decreases the higher mapping rate appeal of the PET assay for these genomes. In this paper, we systematically investigate advantages of the PET assay from a new perspective and demonstrate both experimentally and computationally that it significantly improves the resolution of protein binding site identification. Improving resolution in identifying protein-DNA interaction sites is a critical issue in the study of prokaryotic genomes because prokaryotic transcription factors have closely spaced binding sites, some of which are only 10 to $100bp$ apart from each other [16–19]. These closely spaced binding sites are considered to be multiple "switches" that differentially regulate gene expression under diverse growth conditions [17]. Therefore, identification and differentiation of closely spaced binding sites are invaluable for elucidating the transcriptional networks of prokaryotic genomes.

Although many methods have been proposed to identify peaks from ChIP-Seq data (reviewed in [20]), such as MACS [9], CisGenome [6], and MOSAiCS [10], these approaches reveal protein binding sites only in low resolution, i.e., at an interval of hundreds to thousands of base pairs. Furthermore, they report only one "mode" or "predicted binding location" per peak. More recently, deconvolution algorithms such as CSDeconv [21], GPS [22] (recently improved as GEM [23]), and PICS [11] have been proposed to identify binding sites in higher resolution. However, these methods are specific to SET ChIP-Seq data and are not equipped to utilize the main features of PET ChIP-Seq data. Although a relatively recent method named SIPeS [24] is specifically designed for PET data and is shown to perform better than MACS paired-end mode [9], our extensive computational and experimental analysis indicated that this approach is not

suited for identifying closely located binding events. To address these limitations, we developed dPeak, a high resolution binding site identification (deconvolution) algorithm that can utilize both PET and SET ChIP-Seq data. The dPeak algorithm implements a probabilistic model that accurately describes the ChIP-Seq data generation process and analytically quantifies the differences in resolution between the PET and SET ChIP-Seq assays. We demonstrate that dPeak outperforms or performs competitively with the available SET-specific methods such as PICS, GPS, and GEM. More importantly, dPeak coupled with PET ChIP-Seq data improves the resolution of binding site identification significantly compared to SET-based analysis with any of the available methods. Generation and analysis of σ^{70} factor PET and SET ChIP-Seq data from *E. coli* grown under aerobic and anaerobic conditions reveals the power of the dPeak algorithm in identifying closely located binding sites. Our study demonstrates the importance of high resolution binding site identification when studying the same factor under diverse biological conditions. We further support our findings by validating a small subset of our closely located binding site predictions with primer extension experiments.

Results

Deeply sequenced *E. coli* σ^{70} SET and PET ChIP-Seq data

The σ^{70} factor is responsible for transcription initiation at over 80% of the known promoters in *E. coli* [25]. σ^{70} combines with RNA polymerase to bind promoter sequences typically containing two consensus elements located at $35bp$ and $10bp$ upstream of the transcription start site [18]; thus a σ^{70} binding site spans about $40bp$ upstream from the transcription start site. Many *E. coli* genes contain multiple σ^{70} promoters, and much transcriptional regulation by oxygen as well as by other stimuli occurs by selection of one or a subset of the possible promoters in concert with binding of activators and repressors (e.g., ArcA and FNR for regulation by oxygen [17, 19]). Understanding such regulation requires knowledge of precisely which promoters are used in a given condition. Therefore, the highest possible accuracy of ChIP-signal mapping will allow the best determination of promoter binding by σ^{70}-RNA polymerase holoenzyme.

We generated both PET and SET ChIP-Seq data for σ^{70} factor from *E. coli* grown under aerobic ($+O_2$) and anaerobic ($-O_2$) conditions in glucose minimal media on the HiSeq2000 and Illumina GA IIx platforms. We used these experimental data for comparisons of PET and SET assays and evaluation of our high resolution binding site detection method dPeak throughout the paper. Figure 1B displays PET and SET ChIP-Seq coverage plots for the promoter region of the *cydA* gene under the aerobic condition. The height at each position indicates the number of DNA fragments overlapping that position. The *cydA* promoter contains five known σ^{70} binding sites separated by 11 to $84bp$ [25]. As evidenced in Figure 1B, coverage plots for PET and SET appear almost indistinguishable visually. To further understand the appearance of peaks that multiple binding events in this region would result in, we simulated PET and SET data with parameters matching to those of this region. Figures S1A, B, C in Text S1 display SET and PET coverage plots of this region when it harbors one and three binding events. These plots support that when binding events are in close proximity with distances less than the average library size, they appear as uni-modal peaks regardless of the library preparation protocol (Fig. S1C in Text S1). We next evaluated two peak callers, MACS [11] and MOSAiCS [10], both of which are specifically developed for SET data, on our SET and PET experimental datasets (Table S1 in Text S1). Both methods identified broad regions and the median widths of MACS peaks were 5 to 10 times larger than those of the MOSAiCS peaks. Detailed comparison of the MACS and MOSAiCS peaks revealed that each MACS peak on average has 1.54 to 2.23 MOSAiCS peaks (Table S2 in Text S1). Next, we evaluated the number of annotated σ^{70} binding events from RegulonDB [25] (`http://regulondb.ccg.unam.mx/`) in each of the MACS and MOSAiCS peaks and found that MACS peaks, on average, had 1.86 to 2.02 annotated binding events whereas MOSAiCS peaks had 1.47 to 1.48. Overall, we did not observe any differences

in the peak widths of the PET and SET assays with MOSAiCS whereas MACS peaks from PET data tended to be wider than those of the SET data. These findings indicate that the potential advantages of the PET assay for elucidating closely located binding sites are not simply revealed from visual inspection and by analysis with methods developed specifically for SET data. Hence, deciphering the advantages of PET over SET for high resolution binding site identification warrants a statistical assessment. Next, we developed a generative probabilistic model and an accompanying algorithm, dPeak, that can specifically utilize local read distributions from SET and PET assays. This algorithm enabled unbiased evaluation of the SET and PET assays using our *E. coli* SET and PET ChIP-Seq data.

Analytical framework of the dPeak algorithm

dPeak requires data in the form of genomic coordinates of paired reads (for PET) or genomic coordinates of reads and their strands (for SET) obtained from mapping to a reference genome. For computational efficiency, dPeak first identifies candidate regions (i.e., peaks) that contain at least one binding event and considers each candidate region separately for the prediction of number and locations of binding events (the first step of Fig. 1C). Either two-sample (using both ChIP and control input samples) or one-sample (only using ChIP sample when a control sample is lacking) analysis can be used to identify candidate regions. For this purpose, we utilize the MOSAiCS algorithm [10] which produced narrower peaks than the MACS [11] algorithm in our ChIP-Seq datasets (Table S1 in Text S1).

In each candidate region, we model read positions as originating from a mixture of multiple binding events and a background component (the third step of Fig. 1C). dPeak infers the number of binding events and the read sets corresponding to each binding event within each region. It iterates the following two steps for each candidate region. First, it assigns each read to a binding event or background, based on the positions and strengths of the binding events. Then, the position and strength of each binding event are updated using its assigned reads. In practice, the number of binding events in each candidate region is unknown *a priori*. Hence, we consider models with different numbers of binding events and choose the optimal number using Bayesian information criterion (BIC) [26]. We constructed generative probabilistic models for binding event components and a background component for each of the PET and SET data by careful exploratory analyses of multiple experimental ChIP-Seq datasets. Diagnostic plots of the fitted models (Fig. S3 in Text S1) indicate that the dPeak model fits ChIP-Seq data well.

dPeak has two unique features compared to other peak deconvolution algorithms (Table S3 in Text S1). First, it accommodates both SET and PET data and explicitly utilizes specific features of both types. Second, it incorporates a background component that accommodates reads due to non-specific binding. Consideration of non-specific binding is critical because the degree of non-specific binding becomes more significant as the sequencing depths get larger. An additional unique feature of dPeak is the treatment of unknown library size for SET data. As discussed earlier, to account for unknown library size, each read is either extended to or shifted by an estimate of the library size in most peak calling algorithms [20]. This estimate is often specified by users [7, 10] or estimated from ChIP-Seq data [9, 11]. Currently available algorithms with the exception of PICS use only one extension/shift estimate for all the regions in the genome. However, our exploratory analysis of real ChIP-Seq data and the empirical distribution of the library size from PET data (Fig. S2A in Text S1) indicate that using single extension/shift length might be suboptimal for peak calling (data not shown). In order to address this issue, dPeak estimates optimal extension/shift length for each candidate region. Comparison of empirical distribution of the library size from PET data with the estimates of the region-specific extension/shift lengths indicates that dPeak estimation procedure handles the heterogeneity of the peak-specific library sizes well (Figs. S2B, C, D in Text S1). This advancement ensures that dPeak is well tuned for deconvolving SET peaks, which then enables an unbiased computational comparison between the SET and PET assays.

dPeak outperforms competing methods in discovering closely spaced binding events from SET ChIP-Seq data

We compared dPeak with two competing algorithms, GPS [22] and PICS [11], for analysis of SET ChIP-Seq data. We did not include the CSDeconv algorithm [21] in this comparison because it is computationally several orders of magnitude slower than the algorithms considered here. We utilized the synthetic ChIP-Seq data which was previously used to evaluate deconvolution algorithms [22]. In this synthetic data, binding events were generated by spiking in reads from predicted CTCF binding events at predefined intervals [22] without explicitly implanting binding sequence motifs. Therefore, we also excluded GEM [23], which capitalizes on motif discovery to infer positions of binding events, from this comparison and used additional computational experiments below to perform comparisons with GEM. The synthetic data from [22] consisted of 1,000 joint (i.e., close proximity) binding events, each with two events, and 20,000 single binding events. We assessed performances of algorithms on these two sets separately.

Figure 2A shows the sensitivity of each algorithm at different distances between the joint binding events. Here, sensitivity is the proportion of regions for which both of the two true binding events are correctly identified. dPeak outperforms other methods across all considered distances between the joint binding events and especially for closely located binding events separated by less than the average library size of $250bp$. When the distance between the joint binding events is about $200bp$, dPeak is able to identify both binding events in 80% of the regions whereas neither PICS nor GPS can detect both binding events in more than 20%. Further investigation indicates that PICS merges closely spaced binding events into one event too often (Fig. S4 in Text S1). We also found that GPS estimates the peak shape incorrectly when ChIP-Seq data harbors many closely located binding events (Fig. S5 in Text S1). Furthermore, the sensitivity of GPS also decreases significantly when the distance between joint binding events increases. A closer look at the results reveals that GPS filters out too many predictions for joint binding events.

To ensure that increased sensitivity of dPeak is not a result of increased number of false predictions, we evaluated positive predictive value (fraction of predictions that are correct) of each method. Specifically, we plotted the number of binding events predicted by each algorithm at different distances between the joint binding events in Figure 2B. Since there are two true binding events in each region, two predictions at every distance correspond to perfect positive predicted value. dPeak on average generates more than one prediction and does not over-estimate the number of binding events when the distance between joint events is less than the average library size. This result confirms that the higher sensitivity of dPeak in Figure 2A is not due to increased number of predictions. In contrast, PICS and GPS on average generate only one prediction for closely located binding events, which recapitulates the conclusions from Figure 2A. In summary, dPeak outperforms state-of-the-art deconvolution methods across different distances between joint binding events, especially when the distance between the binding events is less than the average library size.

Next, we evaluated the sensitivity and positive predicted value of the three methods on $20,000$ candidate regions with a single binding event using the additional synthetic data from [22] (Table S4 in Text S1). Average number of predictions per region with at least one predicted binding event and the corresponding standard errors are as follows: dPeak 1.16 (0.42), PICS 1.02 (0.16), GPS 2.72 (1.69). Overall, dPeak slightly over-estimates the number of binding events for regions with a single binding event, and hence PICS is slightly better than dPeak in positive predicted value for these regions. However, as revealed by our joint event analysis, this conservative approach of PICS severely under-estimates the number of binding events when multiple events reside closely. In contrast, GPS significantly under-estimates the number of binding events for the regions with a single binding event since it filters out too many predictions and does not result in a prediction for 82% of the regions. In addition, it over-estimates the number of binding events across regions for which it produces at least one prediction. Comparisons in these two scenarios with and without joint binding events indicate that dPeak strikes a good balance between sensitivity and positive predicted value for both cases.

PET is more powerful than SET for resolving closely spaced binding events

Once we developed dPeak as a high resolution peak detection method for both SET and PET data, we implemented simulation studies to evaluate the PET and SET assays for resolving closely spaced binding events in an unbiased manner. Although SIPeS [24] supports PET ChIP-Seq data, we excluded it from the comparison of PET and SET ChIP-Seq datasets due to its poor performance (Section 16 of Text S1). We generated 100 simulated PET and SET ChIP-Seq data with two closely spaced binding events and evaluated the predictions of these two data types with dPeak (Section 11 of Text S1; Fig. S7 in Text S1).

Figure 2C plots the sensitivity of dPeak as a function of distance between the joint binding events and number of reads for both the PET and SET settings. Note that we evaluated sensitivity up to the distance of $50bp$ because we used $20bp$ windows to determine whether a binding event is correctly identified and as a result, results for the distance less than $50bp$ could be misleading. When the distance between the events is at least as large as the average library size ($\geq 150bp$), the sensitivity using PET and SET data are comparable. However, as the distance between joint binding events decreases, the sensitivity using SET data decreases significantly. In contrast, PET ChIP-Seq retains its high sensitivity even for binding events that are located as close as $50bp$. As the number of reads decreases, sensitivity for both PET and SET data decreases. When there are only 20 DNA fragments (i.e., 40 reads) per binding event, sensitivity for PET data also decreases as the distance between joint binding events decreases. However, even in this case, sensitivity of PET data is still significantly higher than that of SET data with much higher number of reads. Figure 2D displays the number of binding events predicted by dPeak at different distances between joint binding events when 40 reads correspond to each binding event for both PET and SET data and evaluates positive predicted value. Results are similar for higher number of reads (data not shown). With PET ChIP-Seq, dPeak accurately chooses the number of binding events by BIC out of a maximum of five binding events at any distance between the joint binding events. In contrast, SET ChIP-Seq predicts less than two binding events when the distance between the events is less than $150bp$.

We present additional simulation results in Section 10 of Text S1 (Fig. S6 in Text S1). These simulations reveal that even for cases with single binding events, PET has a slight advantage over SET because it predicts the location of the binding event more accurately. Specifically, PET data always provides higher resolution compared to SET data regardless of the strength of the binding event, which we measure by the number of DNA fragments associated with the event. For example, for a binding event with 300 DNA fragments, the average distance between the predicted and true binding events is $0.6bp$ with a standard deviation of $0.8bp$ in the PET data whereas it is $7.6bp$ with a standard deviation of $11.8bp$ in the SET data. Note that although this simulation procedure is based on the assumptions of dPeak model for PET data, our exploratory analysis and goodness of fit (Fig. S3A in Text S1) show that these assumptions hold well in the real PET ChIP-Seq data and therefore, these results have significant practical implications for real ChIP-Seq data.

Analytical investigation with the dPeak generative model explains the difference in sensitivity between PET and SET data

Lower sensitivity of the SET compared to PET data is mainly driven by the loss of information due to unknown library size. We describe this information loss by two concepts named *invasion* and *truncation* (Fig. 3A). Top diagram of Figure 3A depicts two closely spaced binding events and a DNA fragment that is informative for the first binding event (in red) in the PET data. *Invasion* refers to over-estimation of the library size and extension of the read to a length longer than the true one. Equivalently, in the shifting procedure, this corresponds to shifting the read more than necessary. As a result, the read extended to the estimated library size covers both of the closely spaced binding events in the SET data and becomes uninformative or less informative for the binding event it corresponds to. Bottom diagram of Figure 3A also depicts two closely spaced binding events and illustrates *truncation* which we define as

under-estimation of the library size. In this case, the displayed DNA fragment is long and spans both binding events (in red). Therefore, it contributes to estimation of both binding events in the PET data. In contrast, the read extended to estimated library size only covers the first binding event in the SET data and, as a result, its contribution to the first binding event is overestimated whereas its contribution to the second binding event is underestimated. We evaluated the frequency by which fragments with invasion and truncation arise in SET data with a simulation study. Our results (Table S5 in Text S1) indicate that as high as 76.8% and 25.5% of the fragments for a typical peak region can be subject to invasion and truncation with the SET assay.

Figures 3B, C display the probabilities of invasion and truncation, respectively, of a DNA fragment as a function of the distance between binding events and the variance of the library size. The analytical calculations are based on the dPeak generative model (Section 12 of Text S1). Probabilities of invasion and truncation are higher for closely spaced binding events, especially when the library size is shorter than the estimated library size ($150bp$ in this case). In Figure 3B, the probability of invasion decreases for very closely spaced binding events, i.e., when the distance between two binding events is less than $75bp$. As the distance between the binding events decreases, most DNA fragments cover both binding events and the configuration in the first diagram of Figure 3A is unlikely to occur. Hence, there is already insufficient information to predict two binding events even in PET data and relative loss of information (i.e., invasion) in SET data is insignificant. These concepts describe how information on binding events can be lost or distorted by the incorrect estimation of the library size in the SET data. Analytical calculations based on the dPeak generative model show that invasion and truncation influence closely located binding events the most, especially when the library size is not tightly controlled, i.e., exhibit large variation (Figs. 3B, C).

dPeak analysis of σ^{70} PET ChIP-Seq data identifies significantly more RegulonDB supported σ^{70} binding events than the analysis of SET ChIP-Seq data

We compared the performance of PET and SET sequencing for σ^{70} factor under the aerobic condition by generating a 'quasi-SET data' by randomly sampling one of the two ends of each paired reads in PET data and comparing binding events identified from both sets. In order to match number of reads with SET data for fair comparison, only the half number of paired reads was used to construct PET data. Comparison with the quasi-SET data controlled for the differences in the sequencing depths of the original PET and SET samples in addition to the biological variation of the replicates. We then evaluated the dPeak predictions from the PET and SET analyses using the σ^{70} factor binding site annotations in the RegulonDB database as a gold standard. Because a significant number of promoter regions lack RegulonDB annotations, we evaluated the sensitivity based on the regions that contain at least one annotated binding site. This corresponds to 539 binding sites in 363 candidate regions that MOSAiCS identified. Of these 363 regions, 240 harbor only a single annotated binding event. For the regions with more than one annotated binding event, the average distance between binding events is $126bp$. dPeak analysis of the SET data identifies only 38% of the 539 annotated binding events. In contrast, analysis of PET data with dPeak detects 66% of the annotated binding sites. Figure 4A displays average sensitivity as a function of the average distance between annotated binding events for the regions with at least two RegulonDB annotations. A linear line is superimposed to capture the trend for both data types. Notably, the lower sensitivity of SET compared to PET is mainly due to closely located binding events.

We also compared prediction accuracies of the PET and SET assays for the 240 regions that harbor a single annotated binding event. Figure 4B displays resolutions, which we define as the minimum of distances between predicted and annotated positions of binding events, achieved by the PET and SET assays. Median resolutions are $11bp$ (IQR = $16.25bp$) and $28.5bp$ (IQR = $45.25bp$) for PET and SET, respectively. This result indicates that positions of binding events can be more accurately predicted with the PET assay compared to SET even for regions with a single binding event.

To further examine the accuracy of the σ^{70} dPeak predictions, primer extension analysis was performed to map the transcription start site for eight genes (Figs. S10-13 in Text S1; Table S7 in Text S1). dPeak analysis of the PET ChIP-Seq data predicts two closely spaced σ^{70} binding sites in the upstream of each of these eight genes with the distance between predictions ranging $34bp$ to $177bp$. Seven of these predictions are not annotated in RegulonDB and thus represent potential novel transcription start sites. A transcription start site was detected within $21bp$ of 14 (87.5%) of these σ^{70} binding site predictions (Fig. 5A and Table 1), further supporting the accuracy of the dPeak PET predictions.

We treated these 14 validated sites as a gold standard and evaluated the performance of each deconvolution algorithm for these regions. Figure 5B depicts that dPeak with PET ChIP-Seq data attains significantly higher resolution compared to SET-based analysis regardless of the deconvolution algorithm used (p-values of paired t-tests between dPeak using PET data and each of the other methods using SET data are < 0.01). dPeak with SET ChIP-Seq data has a resolution comparable to or better than those of the competing algorithms. GPS is not included in this plot because it provides significantly worse resolution compared to other methods (Fig. S9C in Text S1). Genome-wide comparisons using the RegulonDB transcription start site annotations as a gold standard also lead to a similar conclusion, supporting the notion that PET-analysis with dPeak provides the best resolution (Figs. S9A, B in Text S1).

Figures 4C and 4D display two representative peak regions from these analyses. Figure 4C illustrates two binding events in the promoter regions of *sibD* and *sibE* genes separated by $375bp$. In this case, two peaks are easily distinguishable just by visual inspection and the predictions using both PET and SET data are comparably accurate. Note that although these two binding events are visually distinguishable, standard applications of MACS and MOSAiCS identify this region as a single peak. Widths of MOSAiCS and MACS peaks for this region are $900bp$ and $2,042bp$, respectively. MACS identifies the position of the right binding event as the "summit" of this region (position 3,193,216). Figure 4D displays the promoter region of *yejG* gene, where the distance between the two experimentally validated binding events is only $122bp$. In this case, dPeak application to PET data correctly predicts the number of binding events as two and identifies the locations of these events within $12bp$ of the validated sites. In contrast, all of the SET-based analyses with the deconvolution algorithms (PICS, GPS, GEM) incorrectly predict one binding event located in the middle of the two experimentally validated binding sites.

dPeak analysis of *E. coli* σ^{70} PET ChIP-Seq data identifies closely located binding sites that are differentially occupied between aerobic and anaerobic conditions

High resolution identification of binding sites is especially important for differential occupancy analysis where a protein of interest is profiled under different conditions. Given the high agreement between the dPeak algorithm and experimentally validated transcription start sites at a subset of promoter regions, we set out to identify differential promoter usage between the aerobic and anearobic growth conditions by profiling the *E. coli* σ^{70} factor. Results from the dPeak analysis of the aerobic and anaerobic PET data are summarized in Figure 5C both in the region (i.e., peak) and binding event levels. We identified 868 peaks and 967 dPeak binding events that were common between the $+O_2$ and $-O_2$ conditions. Interestingly, only 82 peaks were unique to the $+O_2$ condition but dPeak analysis identified 247 $+O_2$-specific binding events. Similarly, we identified 130 peaks unique to the $-O_2$ condition while dPeak analysis resulted in 268 $-O_2$-specific binding events. We used the SET ChIP-Seq data from additional biological replicates under both conditions as independent validation of the results. This independent validation using SET data identified 40-60% of the binding events identified by dPeak using PET ChIP-Seq data (56.1% of the common events, 41.3% of the $+O_2$-specific binding events and 42.5% of the $-O_2$-specific binding events). Table S8 in Text S1 further summarizes these results by cross-tabulating the number of predicted binding events in each peak across the two conditions. It illustrates that there are indeed many peaks with at least

one binding event in each condition and different number of binding events across the two conditions. Figure S14 in Text S1 displays an example of closely located binding sites that are differentially occupied between aerobic and anaerobic conditions in σ^{70} PET ChIP-Seq data. These results suggest that dPeak analysis identified many unique σ^{70} binding events that could not be differentiated in the peak-level analysis.

Discussion

High resolution identification of binding sites with ChIP-Seq has profound effects for studying protein-DNA interactions in prokaryotic genomes and differential occupancy. We evaluated PET and SET ChIP-Seq assays and illustrated that PET has considerably more power for deciphering locations of closely spaced binding events. Our data-driven computational experiments indicate that when the distance between binding events gets smaller than the average library size, SET analysis have notably less power than the PET analysis. Furthermore, PET provides better resolution than SET even when a region harbors a single binding event. We developed and evaluated the dPeak algorithm, a model-based approach to identify protein binding sites in high resolution, with data-driven computational experiments and experimental validation. dPeak is currently the only algorithm that can utilize both PET and SET ChIP-Seq data and can accommodate high levels of non-specific binding apparent in deeply sequenced ChIP samples (Table S3 in Text S1). Our data-driven computational experiments and computational analysis of experimentally validated σ^{70} binding sites indicate that it significantly outperforms the currently available PET ChIP-Seq peak finder SIPeS [24]. Application of dPeak to *E. coli* σ^{70} ChIP-Seq data under aerobic and anaerobic conditions revealed that although many peaks identified by standard application of popular peak finders might appear as common between the two conditions, a considerable percentage of these may harbor condition-specific binding events. The high-resolution σ^{70} binding sites identified by dPeak could be combined with start-site mapping or consensus-sequence identification to assign transcriptional orientation to the σ^{70} binding sites.

The advantages of using the dPeak algorithm are not limited to the study of prokaryotic genomes. Applications in eukaryotic genomes include identification of the exact locations of binding motifs when multiple closely located consensus sequences reside in a peak region, studies of *cis* regulatory modules (CRM), and refining consensus sequences. Figure S16 in Text S1 displays an example application of dPeak for differentiating among multiple closely located GATA1 binding sites with consensus WGATAR within a ChIP-Seq peak region critical for erythroid differentiation in mouse embryonic stem cells (data from [27]). CRM studies investigate relationships between spatial configurations of binding sites of multiple transcription factors and gene expression. Relative orders, positions, and distances of binding sites of multiple factors and their relative strengths are key factors in CRM studies [28]. Because dPeak facilitates identification of binding sites of transcription factors in high resolution from ChIP-Seq data, it can enable construction of complex interaction networks among diverse factors across multiple growth conditions.

We evaluated the performance of dPeak on eukaryotic genome ChIP-Seq data that GPS and PICS were optimized for. Figure S17 in Text S1 shows the performance comparison results for transcription factor GABPA profiled in GM12878 cell line from the ENCODE database. It indicates that dPeak performs comparable to or outperforms GPS and PICS. In the case of sequence-specific factors with well-conserved motifs such as the GABPA factor, we observed that dPeak prediction can be further improved in a straightforward way by incorporating sequence information. Figure S17 in Text S1 illustrates that dPeak with incorporated sequence information performs comparable to GEM and identifies the GABPA binding sites with high accuracy.

Recently, ChIP-exo assay [29], a modified ChIP-Seq protocol using exonuclease, has been proposed as a way of experimentally attaining higher resolution in protein binding site identification. Because the ChIP-exo protocol is new and relatively laborious, there are not yet many publicly available ChIP-exo

datasets. We utilized ChIP-exo of CTCF factor in human HeLa-S3 cell line [29] and compared their binding event predictions with dPeak predictions on SET ChIP-Seq data of CTCF in the same cell line. Figure S18 in Text S1 illustrates that dPeak using SET ChIP-Seq data provides higher resolution than ChIP-exo data and that dPeak can be readily utilized for ChIP-exo analysis. Furthermore, it also indicates that dPeak performs comparable to or outperforms currently available methods such as GPS and GEM for both ChIP-exo and SET ChIP-Seq data. Although the real power of the ChIP-exo technique will be revealed as more ChIP-exo datasets are produced and compared with ChIP-Seq datasets, our results with the currently available data suggest that analyzing ChIP-Seq data with powerful deconvolution methods such as dPeak might perform as well as ChIP-exo.

We implemented dPeak as an R package named `dPeak`. `dPeak` utilizes the fast estimation algorithm we developed and parallel computing. Analysis of the σ^{70} data ($\sim 1,000$ candidate regions, each with $\sim 2,300$ reads on average) using our current sub-optimal implementation of `dPeak` takes about 5 minutes using 20 CPUs (2.2 Ghz) when up to 5 binding events are allowed in each candidate region, while it takes about 20 minutes to run `PICS` and `GPS` (also using 20 CPUs). Similarly, analysis of human ENCODE POL2-H1ESC data ($\sim 14,000$ candidate regions, each with ~ 140 reads on average) takes about 10 minutes for `dPeak`, while it takes 100 and 30 minutes for `GPS` and `PICS`, respectively. dPeak is currently available at `http://www.stat.wisc.edu/~chungdon/dpeak/` and will be contributed to public repositories such as Bioconductor [30] and Galaxy Tool Shed [31] upon publication.

Materials and Methods

Growth conditions.

All strains were grown in MOPS minimal medium supplemented with 0.2% glucose [32] at $37°C$ and sparged with a gas mix of 95% N_2 and 5% CO_2 (anaerobic) or 70% N_2, 5% CO_2, and 25% O_2 (aerobic). Cells were harvested during mid-log growth (OD_{600} of ~ 0.3 using a Perkin Elmer Lambda 25 UV/Vis Spectrophotometer). WT *E. coli* K-12 MG1655 ($F-$, $\lambda-$, $rph-1$) was used for the experiments (Kiley lab stock).

ChIP experiments.

ChIP assays were performed as previously described [33], except that the glycine, the formaldehyde, and the sodium phosphate mix were sparged with argon gas for 20 minutes before use to maintain anaerobic conditions when required. Samples were immunoprecipitated using $2\mu L$ of RNA Polymerase σ^{70} antibody from NeoClone (W0004).

Library preparation, sequencing, and mapping of sequencing reads.

For ChIP-Seq experiments, $10ng$ of immunoprecipitated and purified DNA fragments from the aerobic and anaerobic σ^{70} samples (one biological sample for both aerobic and anaerobic growth conditions), along with $10ng$ of input control (two biological replicates for anaerobic Input and one biological sample for aerobic Input), were submitted to the University of Wisconsin-Madison DNA Sequencing Facility for ChIP-Seq library preparation. Samples were sheared to $200-500nt$ during the IP process to facilitate library preparation. All libraries were generated using reagents from the Illumina Paired End Sample Preparation Kit (Illumina) and the Illumina protocol "Preparing Samples for ChIP Sequencing of DNA" (Illumina part # 11257047 RevA) as per the manufacturer's instructions, except products of the ligation reaction were purified by gel electrophoresis using 2% SizeSelect agarose gels (Invitrogen) targeting $275bp$ fragments. After library construction and amplification, quality and quantity were assessed using an Agilent DNA 1000 series chip assay (Agilent) and QuantIT PicoGreen dsDNA Kit (Invitrogen), respectively, and libraries were standardized to $10\mu M$. For PET ChIP-Seq data, cluster generation was performed using an Illumina cBot Paired End Cluster Generation Kit (v3). Paired reads, $36bp$ run was performed for each end, using $200bp$ v3 SBS reagents and CASAVA (the Illumina pipeline) v 1.8.2, on the HiSeq2000. For SET ChIP-Seq data, cluster generation was performed using an Illumina cBot Single Read Cluster Generation Kit (v4) and placed on the Illumina cBot. A single read, $32bp$ run was performed, using standard $36bp$ SBS kits (v4) and SCS 2.6 on an Illumina Genome Analyzer IIx. Base calling was performed using the standard Illumina Pipeline version 1.6. Sequence reads were aligned to the published *E. coli* K-12 MG1655 genome (U00096.2) using the software packages SOAP [34] and ELAND (within the Illumina Genome Analyzer Pipeline Software), allowing at most two mismatches. PET experiments yielded 13.8 million (M) and 22.3M mappable paired 36mer reads and SET yielded 7.4M and 11.5M mappable 32mer reads for aerobic and anaerobic conditions, respectively. Control input experiments, generated with SET sequencing, resulted in 4.6M and 10.2M mappable 32mer reads for the aerobic and anaerobic conditions, respectively. Raw and aligned data files are available at `ftp://ftp.cs.wisc.edu/pub/users/keles/dPeak` and are being processed by GEO for accession number assignment.

dPeak model.

For PET data, if a DNA fragment (paired reads) belongs to g-th binding event, we model its leftmost position conditional on its length L_i as Uniform distribution between $\mu_g - L_i + 1$ and μ_g, where μ_g

is the position of g-th binding event. Lengths of DNA fragments, L_i, are modeled using the empirical distribution obtained from actual PET data. For SET data, if a read belongs to g-th binding event, we model its $5'$ end position conditional on its strand as Normal distribution. Specifically, if a read is in the forward strand, its $5'$ end position is modeled as Normal distribution with mean $\mu_g - \delta$ and variance σ^2. $5'$ end positions for reverse strand reads are modeled similarly with Normal distribution with mean $\mu_g + \delta$ and variance σ^2. Parameters δ and σ^2 are common to all binding event components in each candidate region. Strands of reads are modeled as Binomial distribution. Background reads are assumed to be uniformly distributed over the candidate region that they belong to. Parameters are estimated via the Expectation-Maximization (EM) algorithm [35]. Additional details on the dPeak model and the estimation algorithm for the PET and SET settings are available in Sections 2 and 3 of Text S1.

Method comparison for SET ChIP-Seq data.

We compared the sensitivity and the number of predictions of dPeak with those of PICS [11], GPS [22], and GEM [23]. Sensitivity is the proportion of regions for which both of the two true binding events are correctly identified. A binding event is considered as 'identified' if the distance between the actual binding event and the predicted position is less than $20bp$. Note that we chose a more stringent criteria than the $100bp$ used by GPS for defining true positives because $100bp$ is not high enough resolution for prokaryotic genomes. For the PICS algorithm, we used the R package `PICS` version 1.10, which is available from Bioconductor (`http://www.bioconductor.org/packages/2.10/bioc/html/PICS.html`). For the GPS algorithm, we used its Java implementation version 1.1 from `http://cgs.csail.mit.edu/gps/`. In the performance comparisons using σ^{70} ChIP-Seq data, we also incorporated GEM, a recently modified and extended version of GPS, which incorporates genome sequence of the peaks to improve binding event identification. For the GEM algorithm, we used its Java implementation version 0.9 from `http://cgs.csail.mit.edu/gem/`. We downloaded the synthetic data used for the method comparisons from `http://cgs.csail.mit.edu/gps/` and its description is provided in Supplementary information of the GPS paper [22]. This synthetic data consists of "chrA" with 1,000 regions that harbor two closely spaced binding events and "chrB" to "chrK" with a total of 20,000 regions with a single binding event. We evaluated performances of the methods on joint and single binding event regions separately so that we could assess sensitivity and specificity for each of these cases. dPeak identified candidate regions using the conditional binomial test [6] with a false discovery rate of 0.05 by applying the Benjamini-Hochberg correction [36]. These regions from dPeak were also explicitly provided to the GPS and GEM algorithms as candidate regions. Candidate regions for PICS were identified using the function `segmentReads()` in the `PICS` R package (default parameters). Default tuning parameters were used during model fitting for all the methods.

Simulation studies to compare PET and SET ChIP-Seq data.

We considered distances between binding sites ranging from $50bp$ to $200bp$ which characterize the typical binding event spacing in *E. coli*. We generated and assigned 300 DNA fragments to each of two binding events as follows. For each DNA fragment, we drew the length (L_i) from the distribution of library size, $P(L)$, estimated empirically from the actual σ^{70} PET ChIP-Seq data and group index (Z_i) from multinomial distribution with parameters (0.5, 0.5). Then, for given a library size and group index ($Z_i = g$), leftmost position of the paired reads (S_i) was generated from Uniform distribution between $\mu_g - L_i + 1$ and μ_g, where μ_g is the position of g-th binding event. Rightmost position was assigned as $E_i = S_i + L_i - 1$. SET data was generated by randomly sampling one of two ends from each of these paired reads. For the SET analysis, average library size was assumed to be $150bp$. Then, only half of the total number of paired reads was used to construct PET data, in order to match number of reads with SET data for fair comparison. In addition, we randomly assigned 10 DNA fragments to arbitrary positions within the candidate region to generate non-specific binding (background) reads. The sensitivity and

the number of predictions were summarized over 100 simulated datasets generated by this procedure. A binding event was considered as 'identified' if the distance between the binding event and the predicted position is less than 20*bp*. We repeated these PET versus SET analyses by comparing all the PET data with SET data constructed from selecting one of two ends of each read pair and obtained little or no change in the results (data not shown).

dPeak analysis of σ^{70} PET and SET ChIP-Seq data.

We identified candidate regions, i.e., peaks with at least one binding event, using the MOSAiCS algorithm [10] (two-sample analysis with a false discovery rate of 0.001). In each candidate region, we fitted the dPeak model, which is a mixture of g^* binding event components and one background component (Fig. 1C). In the current analysis, up to five binding event components ($g^{max} = 5$) were considered. The optimal number of binding events was chosen with BIC for each candidate region. We utilized top 50% of the predicted binding events from each condition for the comparison between the aerobic and anaerobic conditions. Overall conclusions remained the same when the full set of predicted binding events are considered.

Primer extension experiments.

Total RNA was isolated as previously described [37]. Oligonucleotide primers (Table S7 in Text S1) were labeled at the 5′ end using [γ-32P]ATP (3,000 $Ci/mmol$) and T4 polynucleotide kinase (Promega) followed by purification with a G25 Sephadex Quick Spin Column (GE). Labeled primer (0.2 $pmol$) was annealed with 7-30 μg total RNA in 20 μl and extended with avian myeloblastosis virus reverse transcriptase (Promega) as described by the manufacturer, except that actinomycin D was present at 100 ug/ml [38]. Primer extension experiments were implemented for *spr* (8 μg $+O_2$ RNA), *dcuA* (8 μg $-O_2$ RNA), *serC* (8 μg $+O_2$ RNA), *aroL* (30 μg and 15 μg $-O_2$ RNA for P_1 and P_2, respectively), *yejG* (30 μg $+O_2$ RNA), *hybO* (30 μg $-O_2$ RNA), *ybgI* (9 μg $+O_2$ RNA), and *ptsG* (9 μg $+O_2$ RNA). A dideoxy sequencing ladder was electrophoresed in parallel with the primer extension products on a 8% (wt/vol) polyacrylamide gel containing 7 M urea. In cases where the transcription start site could be assigned to one of two nucleotides, preference was given to the purine nucleotide.

Software availability.

The dPeak algorithm is implemented as an R package named `dpeak` and is freely available from `http://www.stat.wisc.edu/~chungdon/dpeak/`. We will commit `dpeak` to Bioconductor (`http://www.bioconductor.org`) and Galaxy Tool Shed (`http://toolshed.g2.bx.psu.edu`) upon publication.

References

1. Mikkelsen T, Ku M, Jaffe D, Issac B, Lieberman E, et al. (2007) Genome-wide maps of chromatin state in pluripotent and lineage-committed cells. Nature 448: 553-560.

2. Barski A, Cuddapah S, Cui K, Roh T, Schones D, et al. (2007) High-resolution profiling of histone methylations in the human genome. Cell 129: 823-837.

3. Johnson D, Mortazavi A, Myers R, Wold B (2007) Genome-wide mapping of *in vivo* protein-DNA interactions. Science 316: 1497-1502.

4. Seo Y, Chong H, Infante A, In S, Xie X, et al. (2009) Genome-wide analysis of SREBP-1 binding in mouse liver chromatin reveals a preference for promoter proximal binding to a new motif. Proc Natl Acad Sci USA 106: 13765-13769.

5. Kahramanoglou C, Seshasayee ASN, Prieto AI, Ibberson D, Schmidt S, et al. (2011) Direct and indirect effects of H-NS and Fis on global gene expression control in *Escherichia coli*. Nucleic Acids Res 39: 2073-2091.

6. Ji H, Jiang H, Ma W, Johnson DS, Myers RM, et al. (2008) An integrated software system for analyzing ChIP-chip and ChIP-seq data. Nat Biotechnol 26: 1293–1300.

7. Rozowsky J, Euskirchen G, Auerbach RK, Zhang ZD, Gibson T, et al. (2009) PeakSeq enables systematic scoring of ChIP-seq experiments relative to controls. Nat Biotechnol 27: 66–75.

8. Fullwood M, Wei CL, Liu E, Ruan Y (2009) Next-generation DNA sequencing of paired-end tags (PET) for transcriptome and genome analyses. Genome Res 19: 521–532.

9. Zhang Y, Liu T, Meyer CA, Eeckhoute J, Johnson DS, et al. (2008) Model-based analysis of ChIP-Seq (MACS). Genome Biol 9: R137.

10. Kuan PF, Chung D, Pan G, Thomson JA, Stewart R, et al. (2011) A statistical framework for the analysis of ChIP-Seq data. J Am Stat Assoc 106: 891–903.

11. Zhang X, Robertson G, Krzywinski M, Ning K, Droit A, et al. (2011) PICS: probabilistic inference for ChIP-seq. Biometrics 67: 151–163.

12. Polak P, Domany E (2006) Alu elements contain many binding sites for transcription factors and may play a role in regulation of developmental processes. BMC Genomics 7: 133.

13. Roman AC, Benitez DA, Carvajal-Gonzalez JM, Fernandez-Salguero PM (2008) Genome-wide B1 retrotransposon binds the transcription factors dioxin receptor and Slug and regulates gene expression *in vivo*. Proc Natl Acad Sci USA 105: 1632–1637.

14. Chung D, Kuan PF, Li B, Sanalkumar R, Liang K, et al. (2011) Discovering transcription factor binding sites in highly repetitive regions of genomes with multi-read analysis of ChIP-Seq data. PLoS Comput Biol 7: e1002111.

15. Chen Y, Negre N, Li Q, Mieczkowska JO, Slattery M, et al. (2012) Systematic evaluation of factors influencing ChIP-seq fidelity. Nat Methods 9: 609-614.

16. Bulyk M, McGuire A, Masuda N, Church G (2004) A motif co-occurrence approach for genome-wide prediction of transcription-factor-binding sites in *Escherichia coli*. Genome Res 14: 201–208.

17. Mendoza-Vargas A, Olvera L, Olvera M, Grande R, Vega-Alvarado L, et al. (2009) Genome-wide identification of transcription start sites, promoters and transcription factor binding sites in *E. coli*. PLoS ONE 4: e7526.

18. Reznikoff WS, Siegele DA, Cowing DW, Gross CA (1985) The regulation of transcription initiation in bacteria. Annu Rev Genet 19: 355–387.

19. Ishihama A (2010) Prokaryotic genome regulation: multifactor promoters, multitarget regulators and hierarchic networks. FEMS Microbiology Review 34: 628-45.

20. Wilbanks EG, Facciotti MT (2010) Evaluation of algorithm performance in ChIP-Seq peak detection. PLoS ONE 5: e11471.

21. Lun DS, Sherrid A, Weiner B, Sherman DR, Galagan JE (2009) A blind deconvolution approach to high-resolution mapping of transcription factor binding sites from ChIP-seq data. Genome Biol 10: R142.

22. Guo Y, Papachristoudis G, Altshuler RC, Gerber GK, Jaakkola TS, et al. (2010) Discovering homotypic binding events at high spatial resolution. Bioinformatics 26: 3028–3034.

23. Guo Y, Mahony S, Gifford DK (2012) High resolution genome wide binding event finding and motif discovery reveals transcription factor spatial binding constraints. PLoS Comput Biol 8: e1002638.

24. Wang C, Xu J, Zhang D, Wilson Z, Zhang D (2010) An effective approach for identification of *in vivo* protein-DNA binding sites from paired-end ChIP-Seq data. BMC Bioinformatics 11: 81.

25. Gama-Castro S, Salgado H, Peralta-Gil M, Santos-Zavaleta A, Muniz-Rascado L, et al. (2011) RegulonDB version 7.0: transcriptional regulation of *Escherichia coli* K-12 integrated within genetic sensory response units (Gensor Units). Nucleic Acids Res 39: D98–D105.

26. Schwarz G (1978) Estimating the dimension of a model. Ann Stat 6: 461–464.

27. Wu W, Cheng Y, Keller CA, Ernst J, Kumar SA, et al. (2011) Dynamics of the epigenetic landscape during erythroid differentiation after GATA1 restoration. Genome Res 21: 1659–1671.

28. Noto K, Craven M (2007) Learning probabilistic models of *cis*-regulatory modules that represent logical and spatial aspects. Bioinformatics 23: e156–e162.

29. Rhee HS, Pugh BF (2011) Comprehensive genome-wide protein-DNA interactions detected at single-nucleotide resolution. Cell 147: 1408-1419.

30. Gentleman RC, Carey VJ, Bates DM, Bolstad B, Dettling M, et al. (2004) Bioconductor: Open software development for computational biology and bioinformatics. Genome Biol 5: R80.

31. Goecks J, Nekrutenko A, Taylor J, The Galaxy Team (2010) Galaxy: a comprehensive approach for supporting accessible, reproducible, and transparent computational research in the life sciences. Genome Biol 11: R86.

32. Neidhardt FC, Bloch PL, Smith DF (1974) Culture medium for enterobacteria. J Bacteriol 119: 736–747.

33. Davis SE, Mooney RA, Kanin E, Grass J, Landick R, et al. (2011) Mapping *E. coli* RNA polymerase and associated transcription factors and identifying promoters genome-wide. Method Enzymol 498: 449–471.

34. Li R, Yu C, Li Y, Lam TW, Yiu SM, et al. (2009) SOAP2: an improved ultrafast tool for short read alignment. Bioinformatics 25: 1966–1967.

35. Dempster AP, Laird NM, Rubin DB (1977) Maximum likelihood from incomplete data via the EM algorithm. J R Stat Soc, Series B 39: 1-38.

36. Benjamini Y, Hochberg Y (1995) Controlling the false discovery rate: a practical and powerful approach to multiple testing. J R Stat Soc, Series B 57: 289–300.

37. Khodursky AB, Bernstein JA, Peter BJ, Rhodius V, Wendisch VF, et al. (2003) *Escherichia coli* spotted double-strand DNA microarrays: RNA extraction, labeling, hybridization, quality control, and data management. Methods Mol Biol 224: 61-78.

38. Roth MJ, Tanese N, Goff SP (1985) Purification and characterization of murine retroviral reverse transcriptase expressed in *Escherichia coli*. J Biol Chem 260: 9326-9335.

Figure Legends

Figure 1. SET and PET ChIP-Seq data structure and the dPeak algorithm. (A) Description of paired-end tag (PET) and single-end tag (SET) ChIP-Seq data. Directions of arrows indicate strands of reads. (B) Promoter region of the cydA gene contains five closely spaced σ^{70} binding sites. Blue solid and red dotted curves indicate the number of extended reads mapping to each genomic coordinate in σ^{70} PET and SET ChIP-Seq data, respectively. Black vertical lines mark σ^{70} binding sites annotated in the RegulonDB database. (C) Pictorial depiction of the dPeak algorithm.

Figure 2. Sensitivity and positive predicted value comparisons of high resolution binding site identification algorithms and dPeak performance on PET vs. SET data. (A, B) Comparison of dPeak with PICS and GPS in computational experiments designed for the GPS algorithm. (A) dPeak has higher sensitivity than both PICS and GPS for SET ChIP-Seq data, especially when the distance between binding events is less than the library size. (B) When there are two true binding events in each region, dPeak on average generates more than one prediction and results in a comparable positive predictive value to those of PICS and GPS. PICS and GPS on average generate only one prediction. Shaded areas around each line indicate confidence intervals. (C, D) Comparison of PET and SET assays with dPeak. (C) For SET ChIP-Seq data, the sensitivity of dPeak significantly decreases as the distance between the locations of the events decreases. In contrast, sensitivity from PET ChIP-Seq data is robust to the distance between closely located binding events. The sensitivity for both PET and SET data also decreases as number of reads decreases. (D) dPeak on average predicts two binding events with PET ChIP-Seq data at any distance between the two joint binding events and results in excellent positive predicted value. SET ChIP-Seq data predicts significantly fewer number of binding events as the distance between binding sites decreases. In (C) and (D), n indicates number of reads corresponding to each binding event and $n/2$ DNA fragments are used for PET data to match the number of reads between PET and SET data. (D) shows the case that 40 reads correspond to each binding event and results are similar for other number of reads. Shaded areas around each line indicate confidence intervals.

Figure 3. Illustration of loss of information in SET assay compared to PET assay. (A) Concepts of *invasion* (top diagram) and *truncation* (bottom diagram). In each diagram, the first and second lines indicate PET and SET ChIP-Seq data, respectively. Red horizontal line depicts estimated library size in the SET data. Red circles denote the protein binding event that the read corresponds to. In the case of invasion, this read becomes uninformative regarding the protein binding event whereas with truncation, the read provides incorrect information about the protein binding event. (B) Probability of invasion as a function of distance between binding sites based on the dPeak generative model. (C) Probability of truncation as a function of distance between binding sites based on the dPeak generative model. In (B) and (C), *sigma(L)* refers to estimated standard deviation of the library size distribution in σ^{70} PET ChIP-Seq data and *sigma(L) * a* indicates that the simulation uses standard deviation of *sigma(L) * a* to generate library size. Unshaded areas depict typical range of library sizes.

Figure 4. dPeak analyses and evaluations of σ^{70} PET and SET ChIP-Seq data based on RegulonDB annotated σ^{70} factor binding sites. (A) The numbers of correctly identified binding sites are plotted as a function of the distances between the RegulonDB reported binding events. Linear lines (solid for PET, dashed for SET) through the data points depict general trends. (B) Resolution comparisons of the predictions for the regions with a single annotated binding event. (C, D) PET (blue) and SET (red) coverage plots for representative examples of predicted σ^{70} binding sites. Blue and red dotted vertical lines indicate predictions using PET and SET data, respectively. Black solid vertical lines indicate the annotated binding sites in (C) and experimentally validated binding sites in (D).

Figure 5. Experimental validation and analysis of differential occupancy using dPeak. (A) Validation of a subset of transcription start site predictions using primer extension. Primers (Table S7 in Text S1) complementary to the mRNA sequence $\sim 30 - 50bp$ downstream of each predicted start site were $5'$ end labeled with ^{32}P and 0.2 $pmol$ was used for each 20 μl assay. RNA was isolated from either aerobic ($+O_2$) or anaerobic ($-O_2$) conditions. The sequencing ladders (G, A, T and C) were generated by dideoxy sequencing. Small arrows and filled circles depict the primer extension products. In addition to *dcuA* T_2, a second, less abundant primer extension product (*) was identified with *dcuA* P_2. Since this product was not identified with *dcuA* P_1, it is possible that it corresponds to the start site of an sRNA which terminates upstream of the priming location of P_1. (B) Resolution comparison of the high resolution binding site identification algorithms, using experimentally validated sites as a gold standard (extended version in Figure S9C in Text S1). (C) Summary of the analyses of $+O_2$ and $-O_2$ PET ChIP-Seq data. The 82, 868, and 130 candidate regions (the first diagram) cover 1%, 11%, and 1% of the *E. coli* genome, respectively. In the bottom diagram, the numbers in parentheses depict the set of binding events that were independently validated with predictions from the analysis of biological replicate SET ChIP-Seq.

Tables

Table 1. Experimental validation of the binding events predicted by dPeak analysis of σ^{70} PET ChIP-Seq data.

Gene [a]	Predicted position	True position [b]	Distance	Primer [b]	Condition [c]
yejG	2,276,288	2,276,299	11	P_1	Aerobic
yejG	2,276,432	2,276,419	13	P_2	Aerobic
spr	2,267,945	2,267,942	3	P_1	Aerobic
spr	2,267,825	2,267,833	8	P_2	Aerobic
dcuA	4,364,876	4,364,866	10	P_1	Anaerobic
dcuA	4,364,975	4,364,974	1	P_2	Anaerobic
aroL	405,583	405,579	4	P_1	Anaerobic
aroL	405,489	405,504	15	P_2	Anaerobic
serC	956,823	956,802	21	P_1	Aerobic
serC	956,789	(Not validated)	N/A		Aerobic
hybO	3,144,382	3,144,385	3	P_1	Anaerobic
hybO	3,144,438	(Not validated)	N/A		Anaerobic
ybgI	742,036	742,030	6	P_1	Aerobic
ybgI	741,859	741,874 [d]	15	P_1	Aerobic
ptsG	1,157,005	1,156,989	16	P_1	Aerobic
ptsG	1,156,866	1,156,849 [d]	17	P_1	Aerobic

(a) The genes with promoters harboring the predicted binding events. (b) The true positions were determined by primer extension experiments (Fig. 5A). (c) The conditions under which binding events are validated. (d) We report results based on the RegulonDB annotations for *ybgI* and *ptsG* genes as the primer extension products for these genes were too large to accurately map with the sequencing ladder.

Text S1: Supplementary Methods for "dPeak: High Resolution Identification of Transcription Factor Binding Sites from PET and SET ChIP-Seq Data"

Dongjun Chung[1,#], Dan Park[2], Kevin Myers[2], Jeffrey Grass[3,4], Patricia Kiley[2,4], Robert Landick[3,4,5] & Sündüz Keleş[1,6]

[1] Department of Statistics, University of Wisconsin, Madison, WI, U.S.A.
[2] Department of Biomolecular Chemistry, University of Wisconsin, Madison, WI, U.S.A.
[3] Department of Biochemistry, University of Wisconsin, Madison, WI, U.S.A.
[4] Great Lakes Bioenergy Research Center, University of Wisconsin, Madison, WI, U.S.A.
[5] Department of Bacteriology, University of Wisconsin, Madison, WI, U.S.A.
[6] Department of Biostatistics and Medical Informatics, University of Wisconsin, Madison, WI, U.S.A.
Current address: Department of Biostatistics, Yale University, New Haven, CT, U.S.A.

1 Analysis of the *E. coli* σ^{70} PET and SET ChIP-Seq Data from Aerobic and Anaerobic Conditions by MACS and MOSAiCS

Using MACS (version 1.3.4) and MOSAiCS (version 1.4.0), we performed two sample analysis of the *E.coli* σ^{70} PET and SET ChIP-Seq data (Table S1). For PET ChIP-Seq data, MACS first finds the best pairs of $5'$ and $3'$ reads from multiple alignment results. Then, only the $5'$ read position is kept for every pair and shifted to its $3'$ direction by $100bp$ without estimation of the shift parameter. Then, the

standard MACS analysis [1] is applied to the processed data. In MOSAiCS, when bin-level data are constructed, each read pair is connected and this connected read pair contributes to all the bins it overlaps. The standard MOSAiCS analysis [2] is applied to this bin-level data. Detailed comparison of the MACS and MOSAiCS peaks reveal that each MACS peak on average has 1.54 to 2.23 MOSAiCS peaks (Table S2).

Experiment	PET		SET	
	MACS	MOSAiCS	MACS	MOSAiCS
$+O_2$	270/3202/22	950/450/11.3	534/2550/34	1023/450/11.3
$-O_2$	132/4327/14	993/450/11.8	469/2890/34	1014/450/11.4

Table S1: Analysis of the PET and SET data with MACS and MOSAiCS. Reported numbers a/b/c refer to a: number of peaks; b: median peak width; c: percent genome coverage.

Experiment	Mean (Std)
PET, $+O_2$	1.82 (0.93)
PET, $-O_2$	2.23 (1.10)
SET, $+O_2$	1.54 (0.80)
SET, $-O_2$	1.65 (0.93)

Table S2: Mean number of MOSAiCS peaks overlapping each MACS peak.

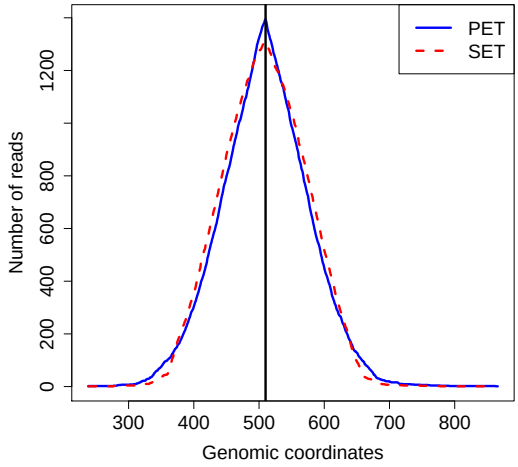

(a)

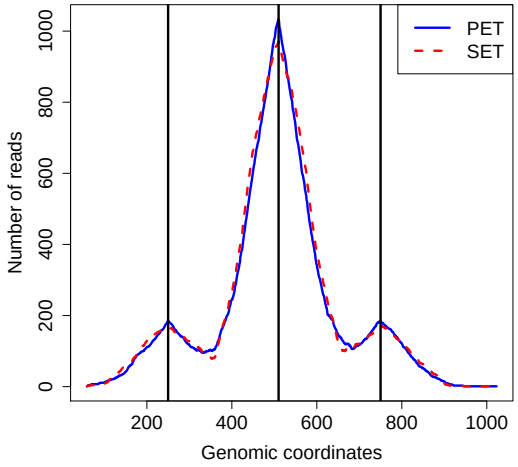

(b)

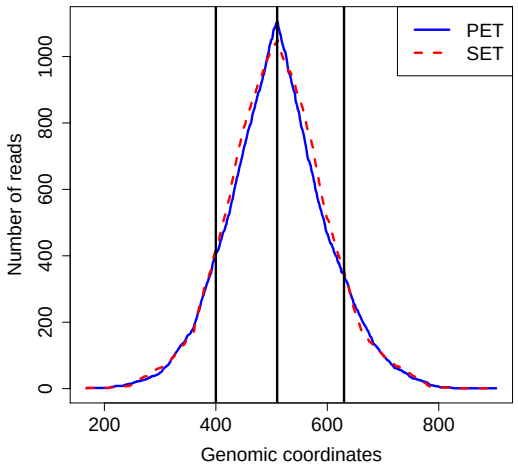

(c)

Figure S1: Coverage plots of simulated read data generated based on cydA promoter parameters estimated by dPeak: (a) single binding event; (b, c) three binding events. dPeak analysis of PET data under aerobic conditions generated three binding event predictions for the cydA promoter region. Consecutive distances between these binding events are 110*bp* and 120*bp*, respectively. The numbers of DNA fragments corresponding to each event are 180, 1035, and 180 (total of 1395), respectively. (a) One simulated binding event (depicted with the black vertical line) with 1395 reads. (b) Three simulated binding events at locations 250, 510, and 750, and with numbers of reads 180, 1035, and 180. (b) Three simulated binding events at locations 400, 510, and 630, and with numbers of reads 180, 1035, and 180.

2 The dPeak Model

Consider a peak with n reads (DNA fragments) and let 1 and m denote the start and end positions of the peak region, respectively. Let g^* denote the number of binding events within the region and μ_g be the position of g-th binding event, $g = 1, 2, \cdots, g^*$. Without loss of generality, assume that $1 \leq \mu_1 < \mu_2 < \cdots < \mu_{g^*} \leq m$ for identifiability. In both PET and SET data, a fraction of reads will denote background noise. We assume that background reads are uniformly distributed over the whole candidate region and denote the background component as $g = 0$.

Let π_g denote the strength of g-th binding event, $g = 0, 1, 2, \cdots, g^*$. π_0 indicates degree of non-specific binding in the candidate region. Let Z_i be the group index of i-th DNA fragment and $Z_i \in \{0, 1, 2, \cdots, g^*\}$. For notational convenience, we denote $Z_{ig} = 1\{Z_i = g\}$, where $1\{A\}$ is an indicator function of event A. We assume that $P(Z_i = g) = P(Z_{ig} = 1) = \pi_g$, $g = 0, 1, 2, \cdots, g^*$ and $\sum_{g=0}^{g^*} \pi_g = 1$. Note that the dPeak model allows each DNA fragment to overlap with multiple binding events. The unobserved Z_i variable ensures that each fragment that is not part of the background overlaps with at least one binding event.

2.1 Generative model for paired-end tag (PET) data

Let S_i and L_i be the start position and length of i-th DNA fragment, respectively. If we denote end position of i-th fragment as E_i, then $E_i = S_i + L_i - 1$ by definition. In the PET data, we directly observe S_i and E_i (equivalently, S_i and L_i) for each DNA fragment. Moreover, distribution of library size, $P(L)$, can be empirically estimated from the PET data and hence, we treat $P(L)$ as known. We denote the whole candidate region as $C = \{2 - L_i \leq S_i \leq m\}$ and the region corresponding to g-th binding event as $B_g = \{\mu_g - L_i + 1 \leq S_i \leq \mu_g\}$. If i-th fragment is generated from g-th binding event ($Z_i = g$), then for given L_i, we assume that S_i is generated from the following Uniform-like distribution:

$$P(s|l; \mu_g, \gamma) = \left[\frac{(1-\gamma)}{l}\right]^{1\{s \in B_g\}} \left[\frac{\gamma}{m-1}\right]^{1\{s \in C \setminus B_g\}},$$

where γ denotes the weight assigned to the area outside of the region corresponding to g-th binding event.

The main purpose to using $P(s|l; \mu_g, \gamma)$ is to make it easier to escape from local maxima during the early iterations of EM algorithm, by making boundaries of B_g "softer" than Uniform distribution. As shown in Section 3.1, γ estimate is essentially obtained as the proportion of DNA fragments that belong to one of the binding

events (i.e., not correspond to background) but do not overlap positions of binding events (μ_g). As iterations progress in the EM algorithm, estimates of μ_g improve and number of such DNA fragments decreases. As a result, in the later iterations of EM algorithm, γ estimate becomes close to zero and $P(s|l;\mu_g;\gamma)$ converges to uniform distribution.

We summarize the fragment generating process as follows:

1. Draw group index of the DNA fragment, $(Z_{i0}, Z_{i1}, Z_{i2}, \cdots, Z_{ig^*})$, from Multinomial$(1, (\pi_0, \pi_1, \pi_2, \cdots, \pi_{g^*}))$.
2. Draw library size, L_i, from known distribution $P(L)$.
3. Draw start position of the DNA fragment, S_i, conditional on Z_i and L_i:
   (a) If the DNA fragment belongs to g-th binding event ($Z_{ig} = 1, 1 \leq g \leq g^*$), draw start position of the fragment, S_i, from $P(S|L;\mu_g,\gamma)$.
   (b) If the DNA fragment is from background ($Z_{i0} = 1$), draw S_i from Uniform$(1-L_i+1, m)$.

2.2 Generative model for single-end tag (SET) data

In the SET data, one of two ends of each DNA fragment is randomly selected and sequenced. Hence, L_i for each fragment is not observable; however, positions and strands of the reads corresponding to the sequenced ends are known (denoted by R_i and D_i, respectively). We assume that D_i follows Bernoulli distribution with known parameter p_D.

Exploratory analysis indicates that these read distributions can be well approximated with Normal distribution. Specifically, we assume that

$$(R|Z = g, D = 1; \mu_g, \delta, \sigma^2) \sim N(\mu_g - \delta, \sigma^2),$$

and

$$(R|Z = g, D = 0; \mu_g, \delta, \sigma^2) \sim N(\mu_g + \delta, \sigma^2).$$

Note that δ corresponds to the half of the distance between modes of the binding event reads in forward and backward strands. We summarize the SET read generating process as follows:

1. Draw group index of the read, $(Z_{i0}, Z_{i1}, Z_{i2}, \cdots, Z_{ig^*})$, from Multinomial$(1, (\pi_0, \pi_1, \pi_2, \cdots, \pi_{g^*}))$.

2. Draw strand of the read, D_i, from Bernoulli(p_D).

3. Draw position of the read, R_i, conditional on Z_i and D_i:

   (a) If the read belongs to g-th binding event ($Z_{ig} = 1, 1 \leq g \leq g^*$) and it is in the forward strand ($D_i = 1$), draw position of the read, R_i, from Normal($\mu_g - \delta, \sigma^2$).

   (b) If the read belongs to g-th binding event ($Z_{ig} = 1, 1 \leq g \leq g^*$) and it in the reverse strand ($D_i = 0$), draw position of the read, R_i, from Normal($\mu_g + \delta, \sigma^2$).

   (c) If the read is from background ($Z_{i0} = 1$) and it is in the forward strand ($D_i = 1$), draw position of the read, R_i, from Uniform($1 - \beta + 1, m$).

   (d) If the read is from background ($Z_{i0} = 1$) and it is in the reverse strand ($D_i = 0$), draw position of the read, R_i, from Uniform($1, m + \beta - 1$).

3 The dPeak Algorithm

We estimate parameters of the models for PET and SET data using the Expectation-Maximization (EM) algorithm [3]. We do not have explicit solutions in the M-step for the PET model. Maximization with respect to $(\mu_1, \mu_2, \cdots, \mu_{g^*})$ requires searching over g^*-dimensional space and $O(m^{g^*})$ operations, which is computationally prohibitive. In order to boost up computation and stabilize estimation, we employ the Expectation-Conditional-Maximization (ECM) algorithm [4]. The ECM algorithm requires only searching over one-dimensional space, $[1, m]$, for the maximization with respect to each μ_g while keeping the other parameters fixed. This reduces the computation time to $O(mg^*)$ operations. Our simulation studies show that this approach is computationally efficient and provides fast convergence with accurate and stable estimation (data not shown). We have explicit solutions in the M-step for the SET model.

Although the EM algorithm has desirable convergence properties, it does not guarantee convergence to the global maximum when there are multiple maxima. As a result, the final estimates depend upon the initial values [5, 6]. In order to address this issue, we consider the stochastic EM algorithm [7], which is a special case of Monte Carlo EM [5, 6], for the first half of iterations. The stochastic EM algorithm allows a chance of escaping from a current path of convergence to a local maximizer to other paths [5]. After certain number of iterations, we switch to the ordinary version of our EM algorithm because the stochastic EM is not desirable when the process is near to convergence to a suitable local maximizer [5].

In the EM implementation, non-identifiability due to overfitting (fitting too many components in the model) is problematic and should be avoided [8, 5]. We address this issue in the during the EM iterations as follows. If the distance between two binding events is shorter than the size of the binding site (defined by the length of the known or predicted consensus motif), we combine these two components and consider it as one component during the remaining iterations. For the σ^{70} application, we set this parameter to $20bp$ since σ^{70} binds to $-35bp$ and $-10bp$ from transcription start site. Moreover, if the strength of a binding event is too weak ($\pi_g < 0.01$), this component is also removed from further consideration in the remaining iterations.

3.1 The dPeak algorithm for PET data

Given the generative model for PET data described in Section 2.1, we have the following complete likelihood:

$$L_C = \prod_{i=1}^{n} P_L(L_i) \left\{ \pi_0 \frac{1\{1 - L_i + 1 \le S_i \le m\}}{m + L_i - 1} \right\}^{Z_{i0}} \prod_{g=1}^{g^*} \left\{ \pi_g \left[\frac{(1-\gamma)}{L_i} \right]^{1\{S_i \in B_g\}} \left[\frac{\gamma}{m-1} \right]^{1\{S_i \in C \backslash B_g\}} \right\}^{Z_{ig}}$$

Let $\mathbf{S} = (S_1, S_2, \cdots, S_n)$, $\mathbf{L} = (L_1, L_2, \cdots, L_n)$, and $\mathbf{\Theta^{(t)}} = \left(\pi_0^{(t)}, \pi_1^{(t)}, \pi_2^{(t)}, \cdots, \pi_{g*}^{(t)}, \mu_1^{(t)}, \mu_2^{(t)}, \cdots, \mu_{g*}^{(t)}, \gamma^{(t)}\right)$. Then, the EM algorithm for the PET data is obtained as follows:

E-step:
For $g = 1, 2, \cdots, g^*$,

$$\begin{aligned} z_{ig}^{(t)} &= E\left(Z_{ig} | \mathbf{S}, \mathbf{L}, \mathbf{\Theta^{(t)}}\right) \\ &= \frac{\pi_g^{(t)}}{A} \left[\frac{(1-\gamma^{(t)})}{L_i} \right]^{1\left\{S_i \in B_g^{(t)}\right\}} \left[\frac{\gamma^{(t)}}{m-1} \right]^{1\left\{S_i \in C \backslash B_g^{(t)}\right\}}, \end{aligned}$$

and for $g = 0$,

$$\begin{aligned} z_{i0}^{(t)} &= E\left(Z_{i0} | \mathbf{S}, \mathbf{L}, \mathbf{\Theta^{(t)}}\right) \\ &= \frac{\pi_0^{(t)}}{A(m + L_i - 1)}, \end{aligned}$$

where A is an appropriate normalizing constant.

M-step:
For $g = 1, 2, \cdots, g^*$, we obtain

$$\mu_g^{(t+1)} = argmax_{\mu_g} \sum_{i=1}^{n} z_{ig}^{(t)} \left[1\{S_i \in B_g\} \log \frac{(1-\gamma^{(t)})}{L_i} + 1\{S_i \in C \backslash B_g\} \log \frac{\gamma^{(t)}}{m-1} \right].$$

and

$$\pi_g^{(t+1)} = \frac{1}{n} \sum_{i=1}^{n} z_{ig}^{(t)}.$$

Similarly,

$$\pi_0^{(t+1)} = \frac{1}{n}\sum_{i=1}^{n} z_{i0}^{(t)}.$$

Moreover,

$$\gamma^{(t+1)} = \frac{1}{n}\sum_{i=1}^{n}\sum_{g=1}^{g^*} z_{ig}^{(t)} 1\left\{S_i \in C \backslash B_g^{(t+1)}\right\}.$$

This algorithm has the following intuitive interpretation. In the E step, each fragment is allocated to a binding event or background component based on whether or not the fragment overlaps the actual binding events. When the fragment overlaps with more than one binding events, it is assigned to each of these events in a fractional manner. The fractions are proportional to relative strengths of the binding events (π_g). In the M step, location of each binding event (μ_g) is essentially updated to the position with the largest number of aligning fragments. In this step, fragments with shorter library size (L_i) have more voting power. This is intuitive from the experimental procedure point of view because it is easier to identify the actual position of a binding event with shorter fragments.

3.2 The dPeak algorithm for SET data

Given the generative model for SET data described in Section 2.2, we have the following complete likelihood:

$$\begin{aligned} L_C = \quad & \prod_{i=1}^{n} \quad \{\pi_0 \left[p_D \frac{1\{1-\beta+1 \le R_i \le m\}}{m+\beta-1}\right]^{1\{D_i=1\}} \\ & \left[(1-p_D)\frac{1\{1 \le R_i \le m+\beta-1\}}{m+\beta-1}\right]^{1\{D_i=0\}}\}^{Z_{i0}} \\ & \prod_{g=1}^{g*} \quad \{\pi_g \frac{1}{\sqrt{2\pi(\sigma^2)}}\left[p_D \exp\left\{-\frac{1}{2(\sigma^2)}(R_i-(\mu_g-\delta))^2\right\}\right]^{1\{D_i=1\}} \\ & \left[(1-p_D)\exp\left\{-\frac{1}{2(\sigma^2)}(R_i-(\mu_g+\delta))^2\right\}\right]^{1\{D_i=0\}}\}^{Z_{ig}} \end{aligned}$$

Let $\mathbf{R} = (R_1, R_2, \cdots, R_n)$, $\mathbf{D} = (D_1, D_2, \cdots, D_n)$, and

$\mathbf{\Theta^{(t)}} = \left(\pi_0^{(t)}, \pi_1^{(t)}, \pi_2^{(t)}, \cdots, \pi_{g*}^{(t)}, \mu_1^{(t)}, \mu_2^{(t)}, \cdots, \mu_{g*}^{(t)}, \delta^{(t)}, (\sigma^2)^{(t)}\right)$. Then, the EM algorithm for the SET data is obtained as follows:

E-step:
For $g = 1, 2, \cdots, g^*$,

$$\begin{aligned} z_{ig}^{(t)} &= E(Z_{ig}|\mathbf{R}, \mathbf{D}, \mathbf{\Theta^{(t)}}) \\ &= \frac{\pi_g^{(t)}}{A\sqrt{2\pi(\sigma^2)^{(t)}}} \left[p_D \exp\left\{-\frac{1}{2(\sigma^2)^{(t)}}(R_i - (\mu_g^{(t)} - \delta^{(t)}))^2\right\}\right]^{1\{D_i=1\}} \\ &\quad \left[(1-p_D)\exp\left\{-\frac{1}{2(\sigma^2)^{(t)}}(R_i - (\mu_g^{(t)} + \delta^{(t)}))^2\right\}\right]^{1\{D_i=0\}}, \end{aligned}$$

and for $g = 0$,

$$\begin{aligned} z_{i0}^{(t)} &= E\left(Z_{i0}|\mathbf{R}, \mathbf{D}, \mathbf{\Theta^{(t)}}\right) \\ &= \frac{\pi_0^{(t)} p_D^{1\{D_i=1\}}(1-p_D)^{1\{D_i=0\}}}{A(m+\beta-1)}, \end{aligned}$$

where A is an appropriate normalizing constant.

M-step:
For $g = 1, 2, \cdots, g^*$, we obtain

$$\mu_g^{(t+1)} = \frac{1}{\sum_{i=1}^n z_{ig}^{(t)}} \sum_{i=1}^n z_{ig}^{(t)} \left[(R_i + \delta^{(t)})1\{D_i = 1\} + (R_i - \delta^{(t)})1\{D_i = 0\}\right],$$

and

$$\pi_g^{(t+1)} = \frac{1}{n}\sum_{i=1}^n z_{ig}^{(t)}.$$

Similarly,

$$\pi_0^{(t+1)} = \frac{1}{n}\sum_{i=1}^n z_{i0}^{(t)}.$$

Moreover,

$$\delta^{(t+1)} = \frac{1}{n}\sum_{i=1}^n \sum_{g=1}^{g^*} z_{ig}^{(t)} \left[(\mu_g^{(t+1)} - R_i)1\{D_i = 1\} + (R_i - \mu_g^{(t+1)})1\{D_i = 0\}\right],$$

and

$$(\sigma^2)^{(t+1)} = \frac{1}{n}\sum_{i=1}^{n}\sum_{g=1}^{g^*} z_{ig}^{(t)} \quad [(R_i - (\mu_g^{(t+1)} - \delta^{(t+1)}))^2 1\{D_i = 1\} + (R_i - (\mu_g^{(t+1)} + \delta^{(t+1)}))^2 1\{D_i = 0\}].$$

This algorithm has the following intuitive interpretation. In the E step, each read is allocated to a binding event or background component based on the distance between the binding events and the read shifted by δ towards its $3'$ direction. Both the peak shape (p_D, δ, and σ^2) and the relative strengths of the binding events (π_g) are considered in this allocation. In the M step, location of each binding event (μ_g) is updated to the averaged position of reads corresponding to the binding event, after they are shifted by δ towards their $3'$ direction. One peak shape is estimated for each candidate region through δ and σ^2. Optimal shift of reads from their corresponding binding events, δ, is updated to the averaged distance between the location of each binding event and the positions of the reads corresponding to this binding event, averaged over binding events in the region. Dispersion of the reads around their corresponding binding events, σ^2, is updated to the variance of the position of reads corresponding to the binding event around location of each binding event (μ_g), after they are shifted by δ to their $3'$ direction, averaged over binding events in the region.

3.3 Model selection.

In practice, determining the optimal number of binding events, g^* in each candidate region can be cast as a model selection problem. Model selection based on the Bayesian Information Criterion (BIC) [9] is a popular choice in mixture modeling and has shown superior performance in diverse applications [10, 11]. Therefore, for pre-specified g^{max}, we fit models for each of $g^* = 1, 2, \cdots, g^{max}$ binding event components and choose the model with the BIC value corresponding to the first local minimum, as the final model.

Choice of g^{max} is an important issue in model selection. g^{max} should be large enough so that all binding events in each candidate region can be considered. On the other hand, setting g^{max} larger than necessary should also be avoided in order to prevent choosing a model due to ill-conditioning rather than a genuine indication of a better model [10, 11]. For appropriate choice of g^{max} in the current application, we checked the number of known binding events in each candidate region of σ^{70} data from the RegulonDB database[12] (`http://regulondb.ccg.unam.mx`) and found that 92% of the peaks have either one or two binding sites within the peak region.

Based on this exploratory analysis, we set $g^{max} = 5$ as the default value and use it for all the analysis described in the manuscript. For other applications, appropriate choice of g^{max} might depend on the protein type and experimental conditions.

4 Estimation of the Optimal Shift in the dPeak Algorithm

Figure S2a displays the density of library size in the σ^{70} PET ChIP-Seq data. The corresponding mean and standard deviations are $192.01bp$ and $26.90bp$, respectively. Figure S2b shows the estimated density of 2δ in the σ^{70} quasi-SET ChIP-Seq data, where δ is the half of the distance between modes of forward and reverse strand reads belonging to each binding event in the candidate region. Mean and standard deviation of 2δ are $187.36bp$ and $9.04bp$, respectively. Figure S2c depicts the scatter plot of library size vs. estimated 2δ and it indicates that, overall, we have larger 2δ estimates for the candidate regions with larger average library sizes. We observe the same pattern in Figure S2d, which displays a similar plot for PET and SET simulation data.

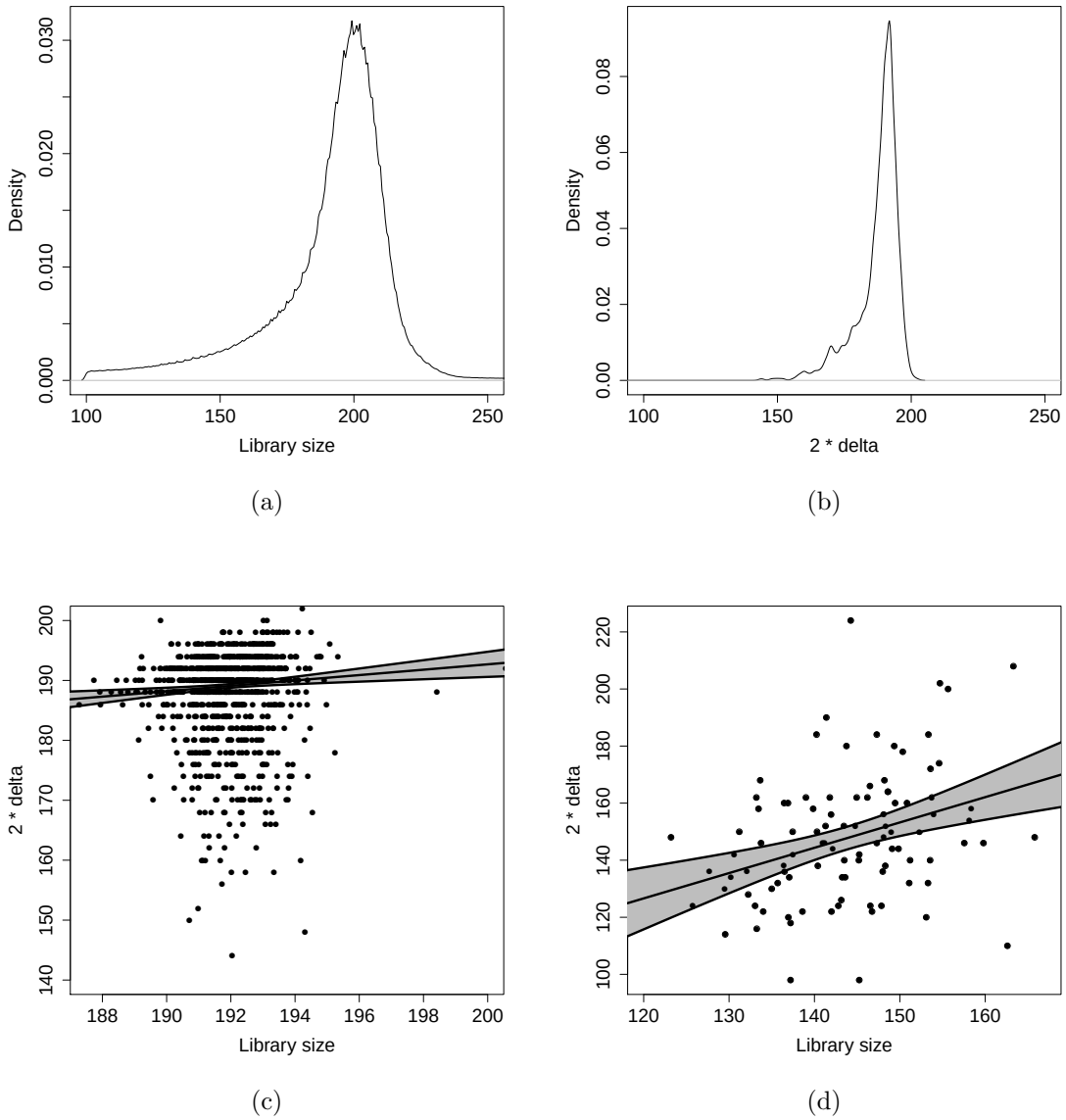

Figure S2: (a) Empirical density of the library size in the σ^{70} PET ChIP-Seq data. (b) Density of estimated 2δ in the σ^{70} quasi-SET ChIP-Seq data. (c) Scatter plot of library size vs. estimated 2δ in the σ^{70} PET and quasi-SET ChIP-Seq data. (d) Scatter plot of library size vs. estimated 2δ in PET and SET simulation data. In (c) and (d), the solid line and shades indicate a robust linear model (RLM) fit and the corresponding confidence intervals, respectively.

5 Diagnostics of the dPeak Model

Figures S3a, b display the goodness of fit (GOF) plots of the analysis displayed in Figure 4C for the PET and quasi-SET ChIP-Seq data, respectively. GOF plots compare the empirical distribution of the read positions with that obtained by simulating from estimated model parameters. These GOF plots are representative of the GOF plots for other candidate regions and they indicate that the dPeak models fit the data well.

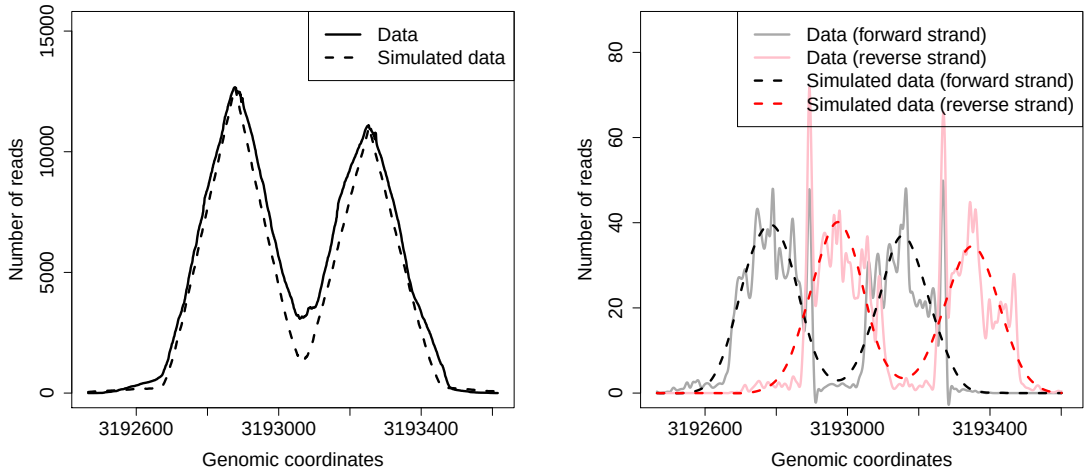

(a) (b)

Figure S3: Goodness of fit (GOF) plot of the analysis displayed in Figure 4C, for (a) the PET and (b) the quasi-SET ChIP-Seq data, respectively.

6 Comparison of deconvolution algorithms

	dPeak	PICS	GPS/GEM[a]
Support PET data	Yes	No	No
Support SET data	Yes	Yes	Yes
Consider non-specific binding	Yes	No	No
Consider local shift of reads	Yes	Yes	No
Construct candidate regions	Utilize both ChIP and control samples	Utilize only ChIP sample	Utilize only ChIP sample
Peak shape estimation	Parametric[b]	Parametric[c]	Nonparametric[d]
Normalization	Normalization using non-specific binding	Normalization by sequencing depth	Regression approach
Merging	No	Yes	No
Filtering	Yes	Yes	Yes
Software interface	R and Galaxy	R	Java
Support parallel computing	Yes	Yes	Yes
Supported aligned read file formats	BED, Eland result, Eland extended, Eland export, Bowtie, SAM	BED, Eland result, Eland export, Bowtie, BAM, SOAP, MAQ[e]	BED, SAM, Bowtie, ELAND, NovoAlign

Table S3: Comparison of deconvolution algorithms. [Note] (a) GEM is a modified and extended version of GPS and it additionally incorporates sequence information to improve identification of binding events. (b) Use Uniform distribution for PET data and normal distribution for SET data, respectively, for binding event components, in addition to Uniform distribution for the background component. (c) Use t-distribution with degree of freedom 4, for binding event components. (d) Requires users provide initial peak shape. (e) File formats supported by `ShortRead` package.

7 Effects of Merging the Step in PICS for Closely Spaced Binding Events

PICS [13] generates initial predictions for locations of protein binding events and then merges initial predictions that have overlapping "binding event neighborhoods". A binding event neighborhood is defined as the predicted location of a binding event extended by three standard errors of the shift parameter estimate to both sides. In order to evaluate the effect of merging on PICS binding event predictions, we re-generated results in Figures 2A, B without the merging step for PICS. Figures S4a, b show that PICS without merging step performs comparable to dPeak for SET ChIP-Seq data and the merging step of PICS results in loss of resolution for closely spaced binding events. Although it might be possible to tune the merging step, PICS currently does not provide this functionality.

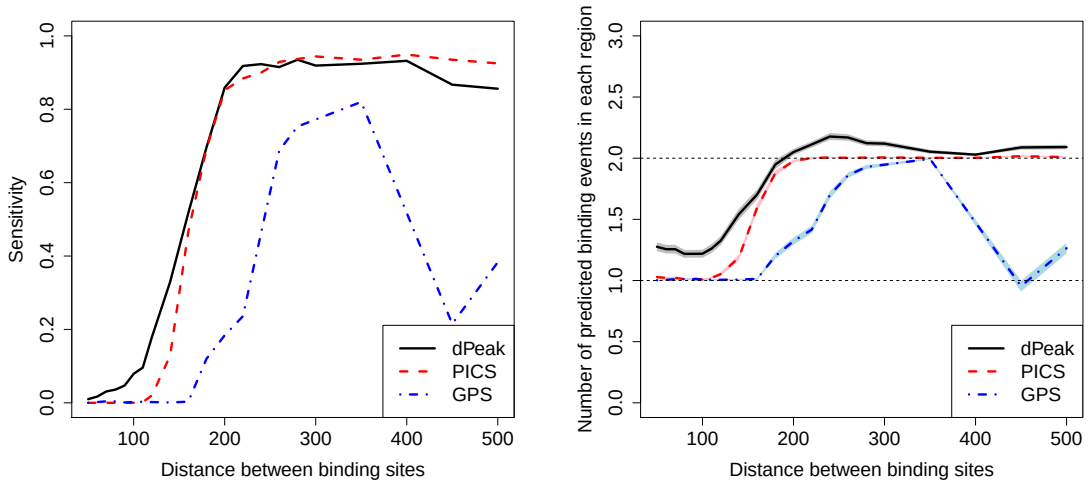

(a) (b)

Figure S4: Sensitivity (a) and positive predicted value (b) comparisons of high resolution binding site identification methods in computational experiments designed for the GPS algorithm. In these evaluations, the merging step is skipped in PICS as opposed to the evaluations obtained by default parameters of PICS in Figures 2A, B of the main text.

8 Peak Shape Estimation of GPS for Closely Spaced Binding Events

Figure S5a displays the peak shape estimated by the GPS algorithm [14] for synthetic ChIP-Seq data when there is only one binding event in each candidate region. It depicts density of forward strand reads with respect to the distance from the location of binding event (corresponding to zero in the x axis). This same peak shape is used genome-wide for modeling of reads in both forward and reverse strands. When there is single binding event, peak shape is correctly estimated as uni-modal. Figure S5b displays the peak shape when the distance between two binding sites in each candidate region is set to $450bp$. The peak shape is still correctly estimated as uni-modal and it looks similar to the peak shape estimated for single binding events. Moreover, in these two cases, the estimated peak shapes are similar to their initial shapes. Figure S5c shows the estimated peak shape when the distance between two binding sites in each candidate region is set to $140bp$. In this case, both of the two closely spaced binding events affect peak shape estimation of the GPS algorithm. As a result, the peak shape is estimated bi-modal, which in turn leads to predicting the two binding events as a single event after a few rounds of the GPS iterations. We note that this problem typically occurs for nonparametric mixture models when the distances between mixture components are relatively short compared to the bandwidth.

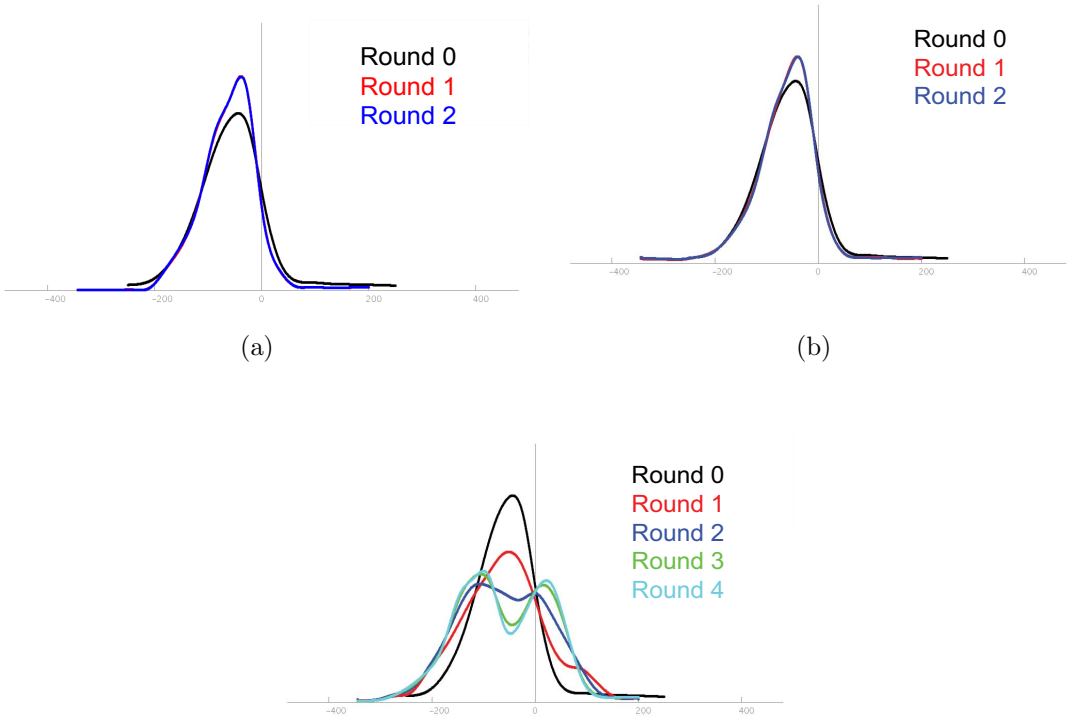

Figure S5: Peak shapes estimated by the GPS algorithm for synthetic ChIP-Seq data: (a) when there is a single binding event; (b, c) when the distance between joint binding events is set to 450*bp* (b) and 140*bp* (c). "Round" denotes the iteration number in the algorithm and "Round 0" depicts the initiation.

9 Evaluations on Synthetic Data from [14] with a Single Binding Event

# of predicted events	0	1	> 1	Average # of events
dPeak	0%	86 %	14%	1.16 (0.42)
PICS	1%	97%	2%	1.02 (0.16)
GPS	82%	6%	12%	2.72 (1.69)

Table S4: Prediction accuracy for $20,000$ candidate regions with single binding event. Columns 2-4 report percentages of candidate regions with various numbers of predicted binding events. Column 5 reports the average number of binding events across regions with at least one predicted binding event.

10 Evaluations on Simulation Data with Single Binding Events

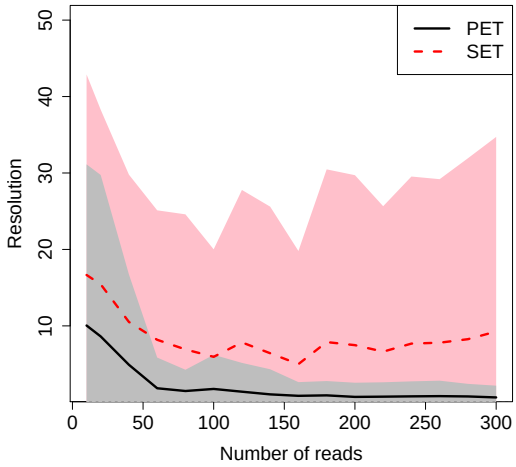

Figure S6: Resolution of predictions as a function of number of DNA fragments in PET and SET simulated data with a single binding event. Resolution is defined as the absolute distance between the predicted and true binding event positions. Black solid and red dotted curves indicate averaged resolutions for each number of DNA fragments in PET and SET data, respectively. Gray and pink shades indicate their confidence intervals in PET and SET data, respectively.

11 Evaluations on Simulation Data based on Different Data Generation Process

When comparing PET and SET data with simulations (Figs. 2C, D and Fig. S6), we first generated PET data and then obtained corresponding SET data by randomly sampling one of two ends of each resulting DNA fragment. Although such a data generation process closely mimics the process for generating real SET ChIP-Seq data, dPeak model for SET ChIP-Seq data capitulates this process by a Normal approximation of the density of each of forward and reverse strand reads. In order to assure that our evaluation using random sampling does not give unwarranted advantages to PET data, we generated SET data with read positions directly originating from Normal distribution and repeated the analysis in Figures 2C, D. Figures S7a, b, c confirm that the comparisons between PET and SET data remain the same regardless of how SET data is simulated.

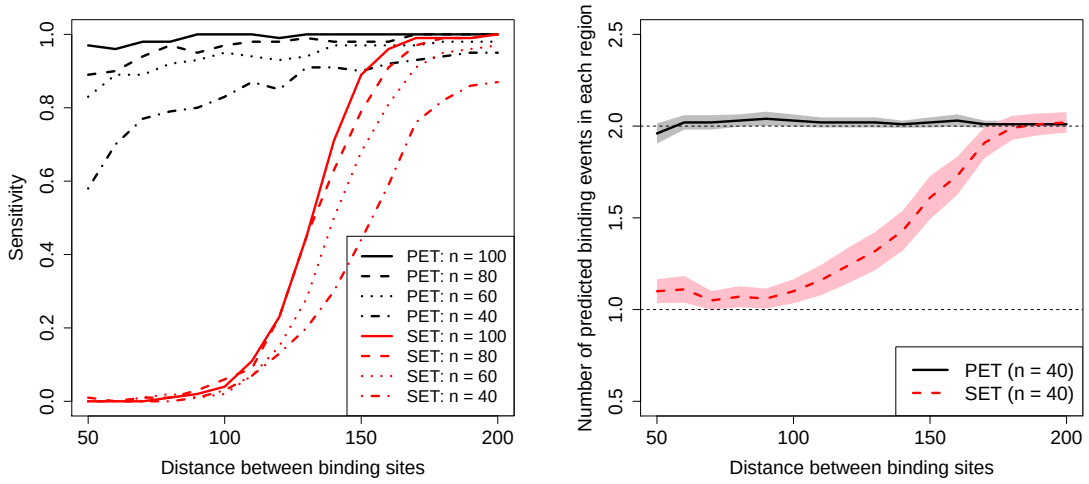

(a) (b)

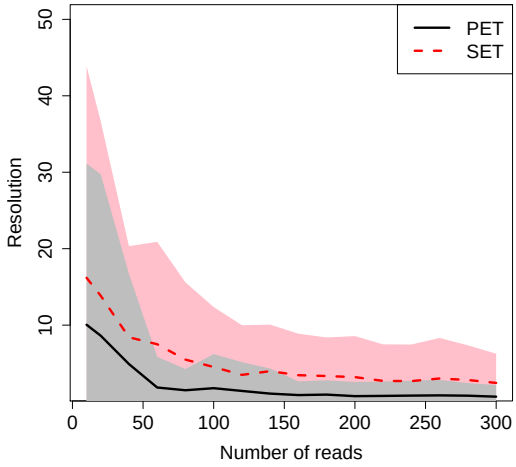

(c)

Figure S7: Sensitivity (a), positive predicted value (b), and resolution (c) comparisons of dPeak performance on PET vs. SET data when SET read density is directly generated from Normal distribution. n indicates number of reads corresponding to each binding event and $n/2$ DNA fragments are used for PET data to match the number of reads between PET and SET data. Shaded areas around each line indicate confidence intervals. Results are similar to those in Figures 2C, D, and Figure S6, where SET data is generated by random sampling of one of the two ends from each DNA fragment in PET data.

12 Analytical Calculations for Invasion and Truncation

Consider a region with two closely located binding events. Processing of DNA fragments generated from this region will lead to classification of the fragments in one of the following four categories:

Category I: Fragments overlapping a single true binding event.

Category II: Fragments overlapping both binding events.

Category III: Fragments overlapping only the false binding event.

Category IV: Fragments not overlapping any binding events.

Only fragments in category I are truly informative. Fragments in category II are less informative than fragments in category I. They could potentially contribute to both binding events, possibly through proportional allocation based on relative distances from each binding event. However, ambiguity in prediction increases as the number of fragments in category II increases. Fragments in category III introduce noise to binding event estimation since they are associated with the wrong binding event. Fragments in category IV are uninformative. In summary, invasion refers to increased number of category II fragments in SET data compared to PET data and truncation refers to increased number of category III and IV fragments in SET data compared to PET data.

Table S5 displays the number of fragments in each category from one simulated dataset where we set the distance between the two binding events as $50bp$. Average library size is $139bp$ in the PET data. The estimated library size used with SET analysis are reported in parentheses in the first column. In the corresponding SET data, even when extension is relatively accurate (extension = $150bp$), numbers of fragments in categories II to IV increase significantly compared to PET data. When the library size is under-estimated as $100bp$, we have significantly more fragments in categories III and IV (truncation; Fig. S8b). In contrast, when it is over-estimated as $200bp$, we have significantly more fragments in category II (invasion; Fig. S8a).

We used the dPeak generative model and calculated the probability of invasion and truncation (Fig. S8) as follows. As in the previous sections, let S and L be start position of DNA fragment and its length, respectively, in PET ChIP-Seq data. Let l^* denote the fixed library size used in the analysis of SET ChIP-Seq data. Z indicates group index of the DNA fragment where $Z = 1$ and $Z = 2$ indicates correspondence to the first and second binding events, respectively. Let μ_1 and μ_2 be positions of

Category	I	II	III	IV
	Informative	Less informative		
	Overlapping only true binding events	Overlapping both binding events	Overlapping only false binding event	Not overlapping any binding event
PET	225	375	0	0
SET (150)	174	391	19	16
SET (100)	232	215	89	64
SET (200)	133	461	3	3

Table S5: Classification of 600 DNA fragments from one simulated dataset with two binding events separated by $50bp$.

first and second binding events, respectively, and assume that $\mu_1 < \mu_2$. Probability of invasion (Fig. S8a) is obtained as:

$$\begin{aligned} P(Invasion) &= E_L[P(S < \mu_1 < S + L < \mu_2 < S + l^* | Z = 1)] \\ &= \sum_{L=l} P(L = l) P(S < \mu_1 < S + l < \mu_2 < S + l^* | Z = 1, L = l) \\ &= \sum_{L=l} P(L = l) min\left\{l, \mu_2 - \mu_1, l^* - l, l^* - (\mu_2 - \mu_1)\right\} / l. \end{aligned}$$

As illustrated in Figure S8b, for truncation, we consider the case that the original DNA fragment covers both binding events in PET data. The corresponding probability can be calculated by defining the truncation event with the use of the Z variable:

$$\begin{aligned} P(Truncation) &= E_L[P(S + l^* < \mu_2, S < \mu_1 < \mu_2 < S + L | Z = 2)] \\ &= \sum_{L=l} P(L = l) P(S + l^* < \mu_2, S < \mu_1 < \mu_2 < S + l | Z = 2, L = l) \\ &= \sum_{L=l} P(L = l) min\left\{l - l^*, l - (\mu_2 - \mu_1)\right\} / l. \end{aligned}$$

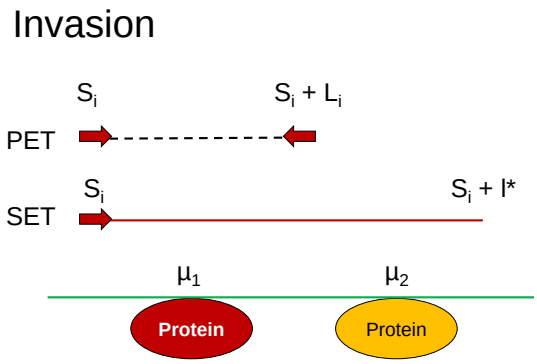

(a)

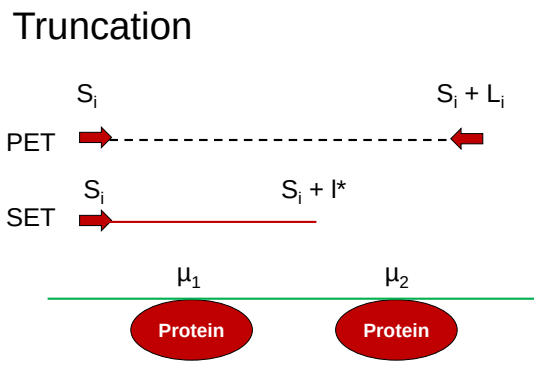

(b)

Figure S8: Concepts of (a) *invasion* and (b) *truncation*. In each diagram, the first and second lines indicate PET and SET ChIP-Seq data, respectively. Red horizontal line depicts estimated library size in the SET data. Red circles denote the protein binding event that the read corresponds to.

13 Evaluations on σ^{70} PET and SET ChIP-Seq Data Using RegulonDB and Experimentally Validated Sites as a Gold Standard

We compared performances of deconvolution algorithms dPeak, PICS, GPS, and GEM using σ^{70} PET and quasi-SET ChIP-Seq data by considering RegulonDB annotated binding sites as a gold standard. As discussed in the main text, quasi-SET ChIP-Seq data obtained by randomly selecting one end of each fragment from PET data avoided issues like differences in sequencing depths, technical, and biological variability. We assessed sensitivity of each algorithm using the set of candidate regions with at least two annotated binding sites and evaluated resolution using the candidate regions with exactly one annotated binding site.

Table S6 and Figures S9a, b show that dPeak using PET ChIP-Seq data provides significantly higher sensitivity and resolution than SET ChIP-Seq data regardless of the deconvolution algorithm used. GPS performs the worst and its poor performance had recently motivated the development of GEM [15]. Overall, dPeak and GEM perform similarly and both are slightly better than PICS with SET data in terms of sensitivity.

We also compared deconvolution algorithms using our small set of experimentally validated binding sites as a gold standard. This comparison (Fig. S9c) further confirmed our conclusions from the RegulonDB-based comparisons. The differences in resolution between dPeak using PET ChIP-Seq data and each of the deconvolution algorithms using SET ChIP-Seq data are statistically significant with p-values $<$ 0.01.

	dPeak (PET)	dPeak (SET)	PICS	GPS	GEM
$+O_2$	0.66	0.47	0.39	0.20	0.43
$-O_2$	0.64	0.43	0.41	0.10	0.47

Table S6: Sensitivity comparisons across regions with at least two annotated binding events for σ^{70} PET and quasi-SET ChIP-Seq data in aerobic and anaerobic conditions. RegulonDB annotated binding sites are used as a gold standard. A gold standard binding event is marked as identified if the distance between the prediction and the RegulonDB reported location is less than $30bp$ (overall conclusions remained the same with other distances).

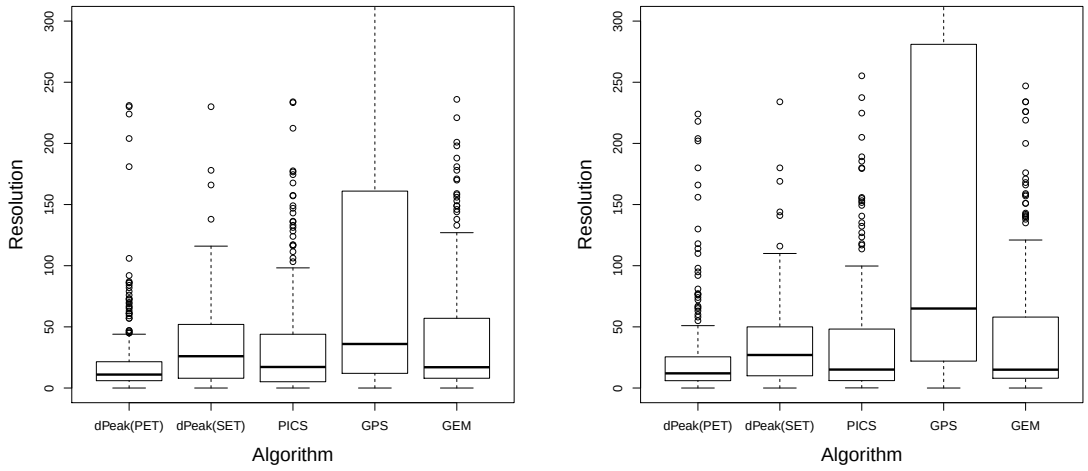

(a)

(b)

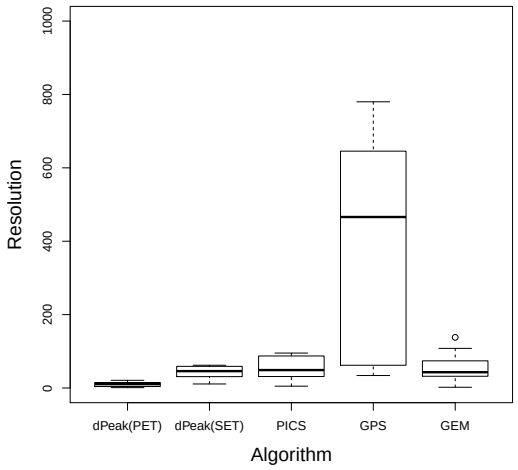

(c)

Figure S9: Resolutions of predictions for the regions with a single annotated binding event for σ^{70} PET and quasi-SET ChIP-Seq data in aerobic (a) and anaerobic (b) conditions when RegulonDB annotated binding sites are used as a gold standard. (c) Resolutions of predictions for σ^{70} PET and quasi-SET ChIP-Seq data using experimentally validated binding sites as a gold standard.

14 Experimental Validation of dPeak Predictions from σ^{70} PET ChIP-Seq Data

Name	DNA sequence
yejGP1	GGACGATTGAGAGTTGTAATG
yejGP2	CCTCTATGGCTCTGATTTAAG
sprP1	GTTTGTTTTCCCTTGAAGTCC
sprP2	CCAAATCTGTGGACTAACGCA
dcuAP1	GCATATTAGCCTTCCTTGTT
dcuAP2	CCCTGTACGATTACTGTTCG
serCP1	TTGAAGATTTGAGCCATTTCC
aroLP1	AAAGAGGTTGTGTCATCGTG
aroLP2	GCGATCATACCATCAAACTAG
hybOP1	CAATAATGCGATCGATGCGCC
ybgIP1	CGTTAATCAGTTGTTCCAGT
ptsGP1	TCCTGAGTATGGGTGCTTT

Table S7: Primers.

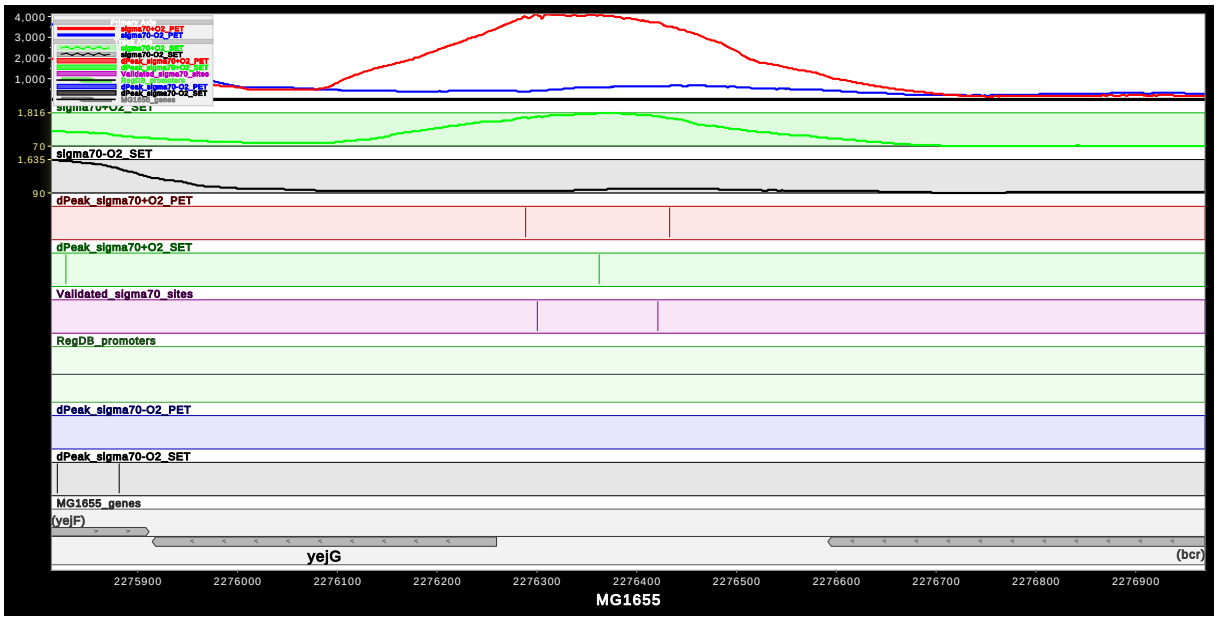

(a)

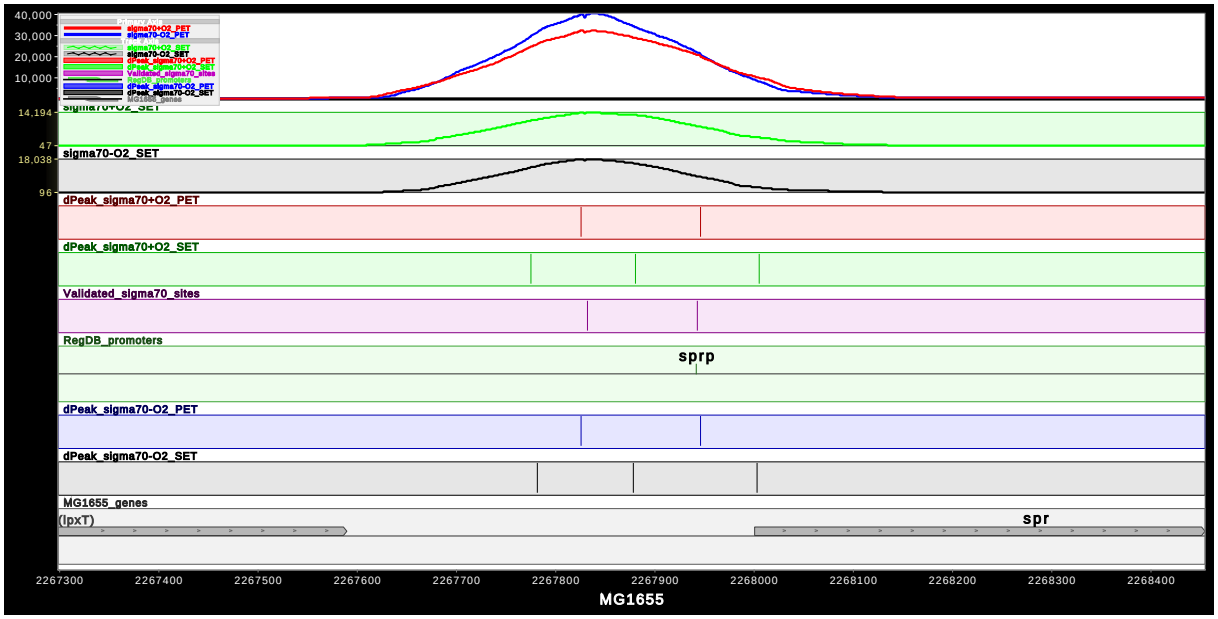

(b)

Figure S10: MochiView genome browser [16] screenshots of promoter regions of *yejG* (a) and *spr* (b) genes.

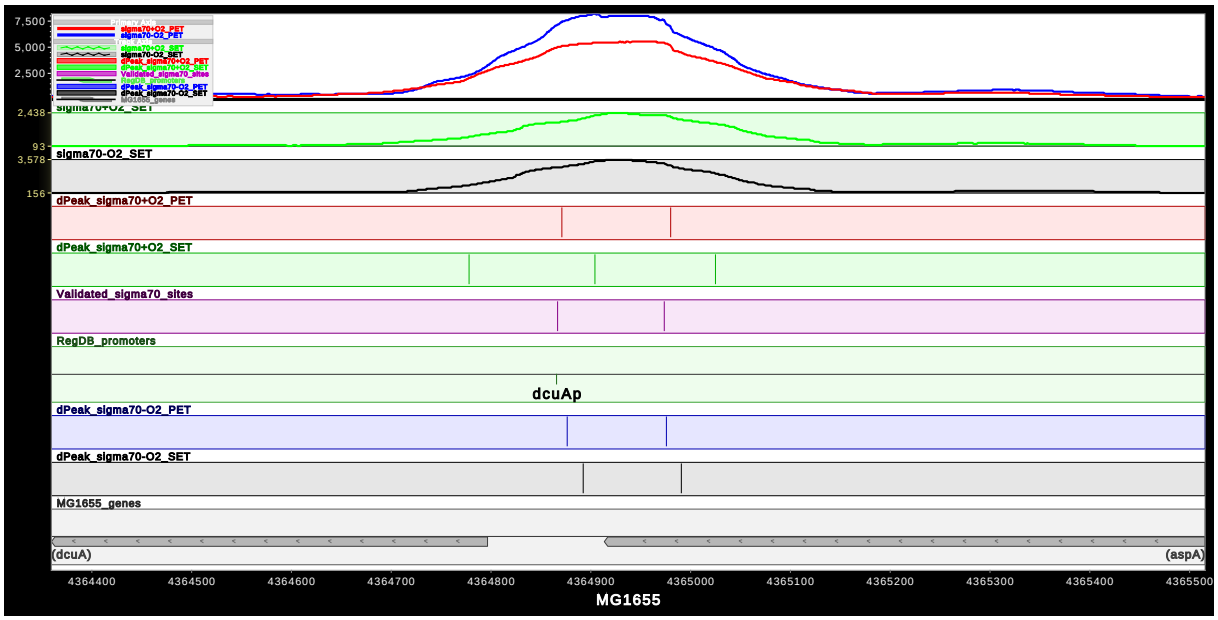

(a)

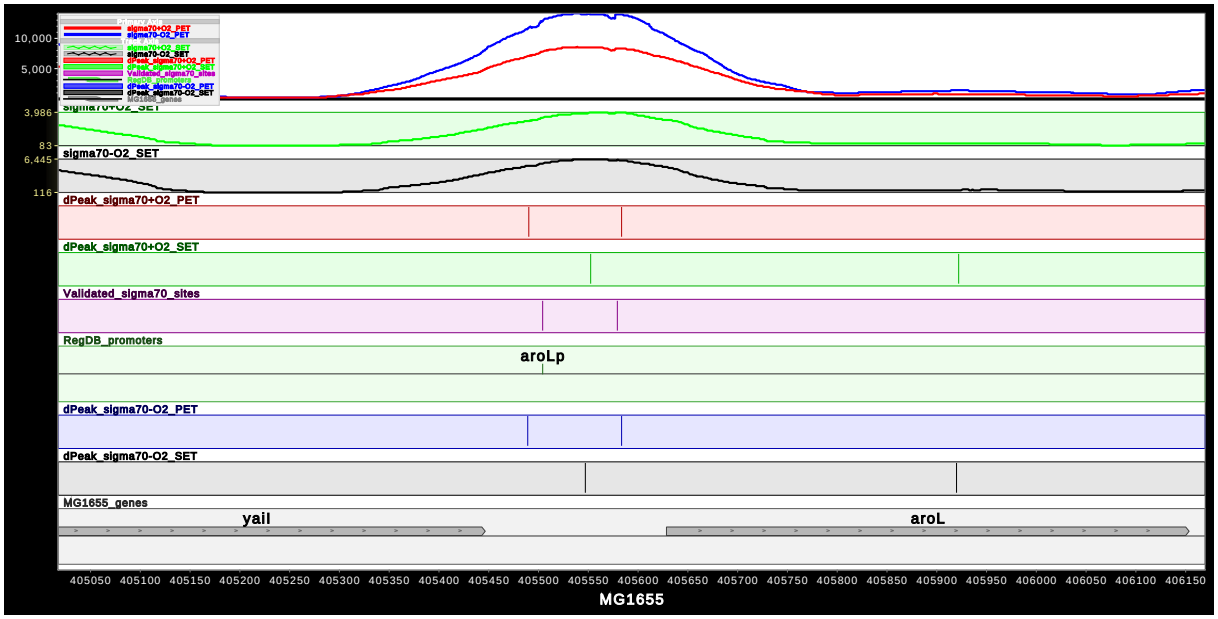

(b)

Figure S11: MochiView genome browser [16] screenshots of promoter regions of *dcuA* (a) and *aroL* (b) genes.

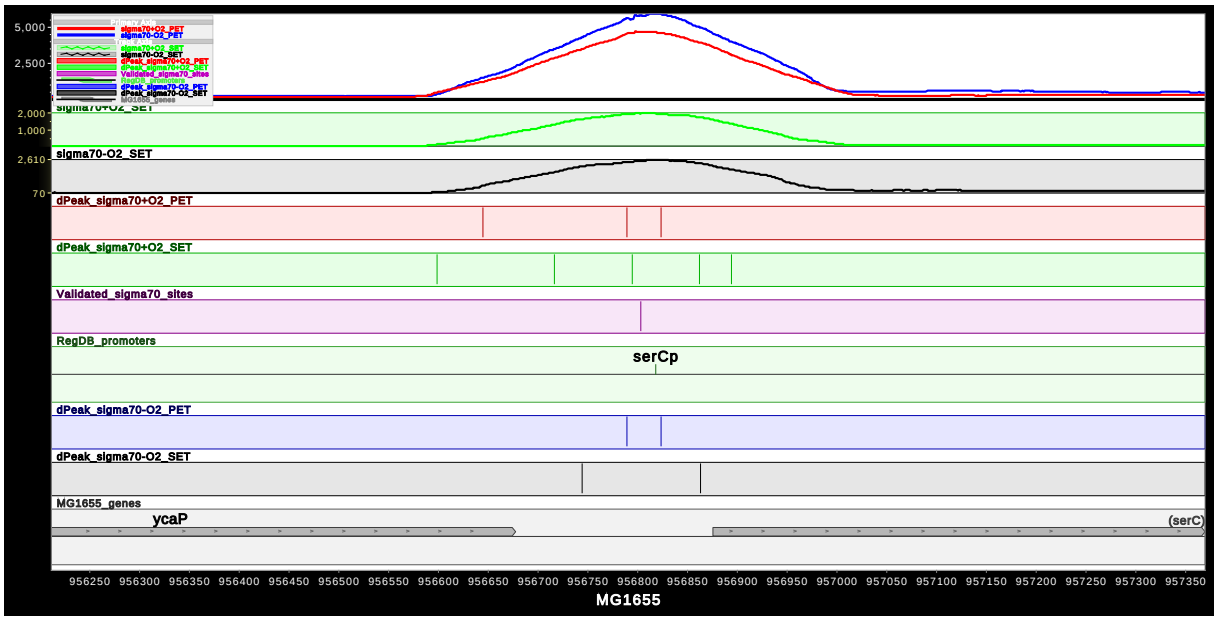

(a)

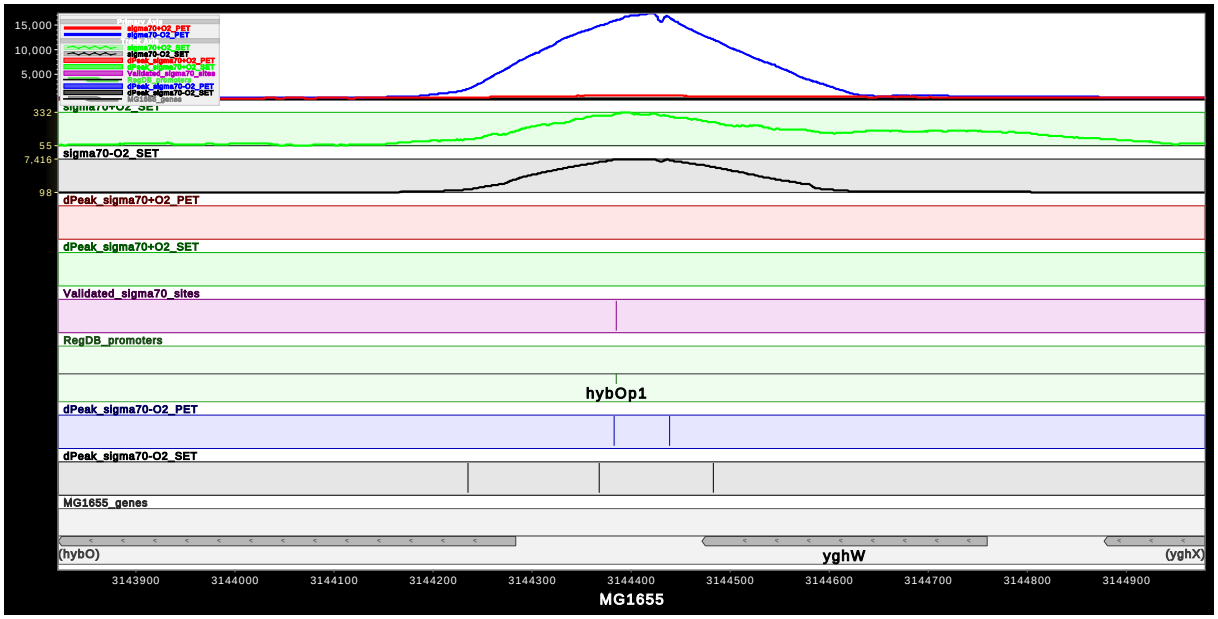

(b)

Figure S12: MochiView genome browser [16] screenshots of promoter regions of *serC* (a) and *hybO* (b) genes.

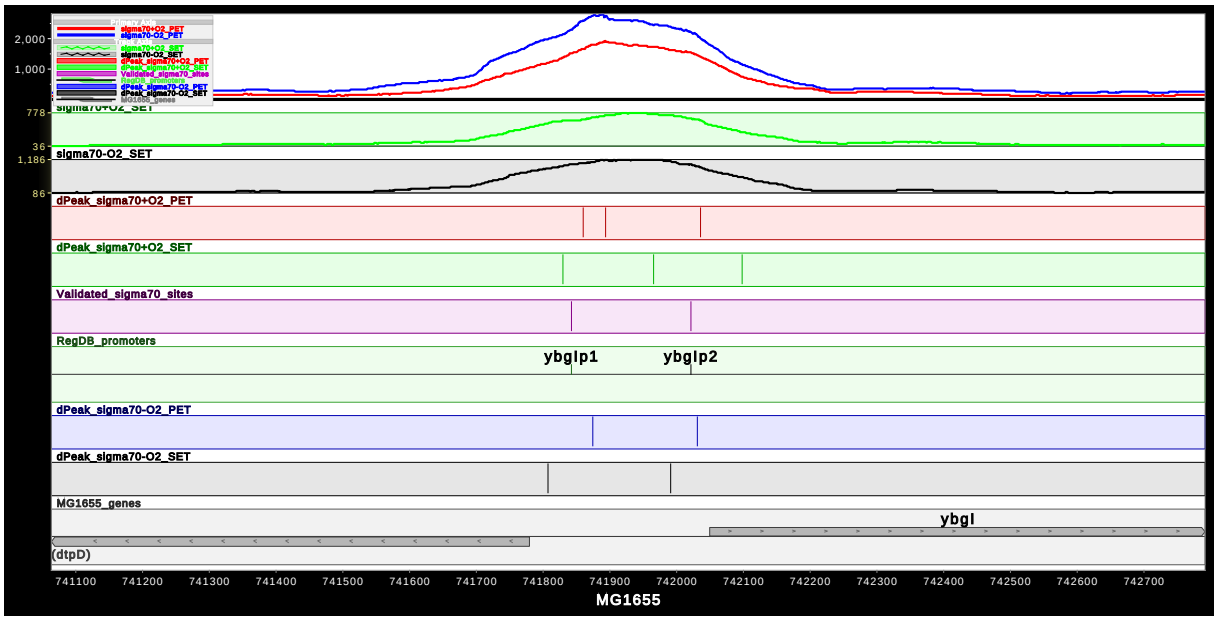

(a)

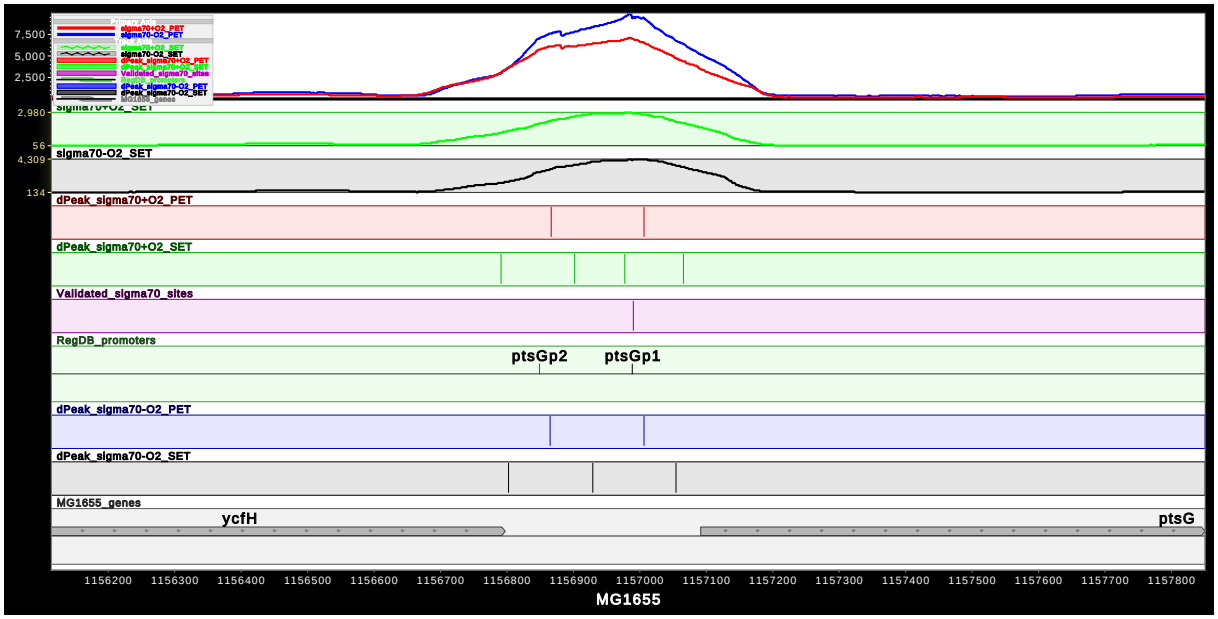

(b)

Figure S13: MochiView genome browser [16] screenshots of promoter regions of *ybgI* (a) and *ptsG* (b) genes.

15 Differential occupancy of closely located binding sites between aerobic and anaerobic conditions in *E. coli* σ^{70} PET ChIP-Seq data

Figure 5C elucidates the merit of high resolution analysis in the studies of differential occupancy. However, if there is no occupancy in one condition at all, such differential binding could still be identified in the peak-level analysis and high resolution analysis might be considered less interesting. High resolution analysis is perhaps most interesting when the same region is identified as a peak in both conditions but different numbers of binding events are identified between conditions. We further decomposed the predicted binding events based on the number of predicted events in the region in each condition. Table S8 shows that although many regions are occupied in both conditions, the number of predicted binding events can differ significantly. Figure S14 depicts an example of differential occupancy of closely located binding sites in the promoter region of *gltA* gene. Specifically, two binding sites are predicted by dPeak in anaerobic condition while only one of them are identified in aerobic condition. In contrast, MOSAiCS identified the region covering both binding sites as a single peak in both aerobic and anaerobic conditions.

	Anaerobic condition			
Aerobic condition	0	1	2	≥ 3
0	N/A	60	19	1
1	63	198	74	7
2	16	48	235	34
≥ 3	1	3	24	30

Table S8: Cross tabulation of number of binding events for each peak of σ^{70} PET ChIP-Seq data between aerobic and anaerobic conditions.

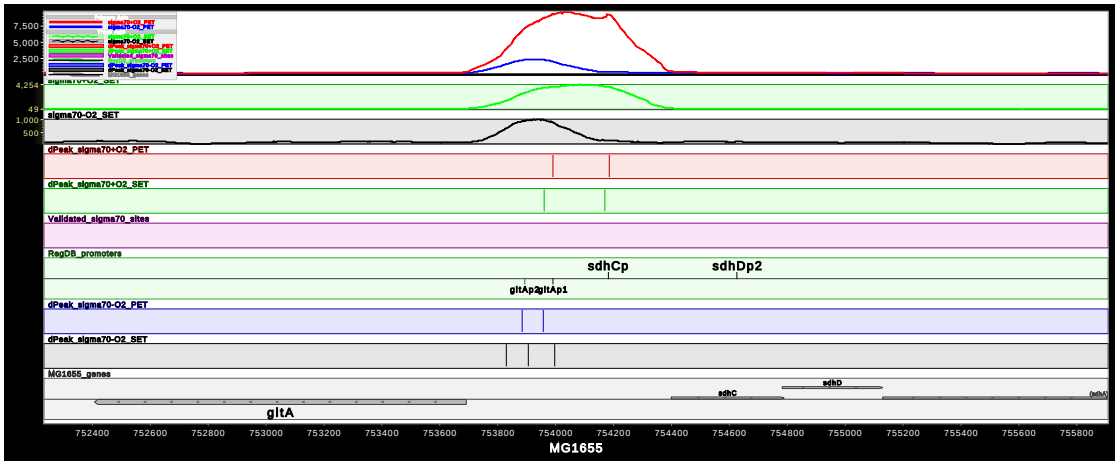

Figure S14: MochiView genome browser [16] screenshots of promoter region of *gltA* gene. Both *gltAp1* and *gltAp2* are identified as binding sites in anaerobic condition using PET ChIP-seq data while only *gltAp1* is identified in aerobic condition.

16 Evaluations of the Algorithms for PET ChIP-Seq Data

To the best of our knowledge, SIPeS is currently the only algorithm specifically designed for supporting PET ChIP-Seq data and has been shown to attain better resolution than a version of MACS that can analyze PET data [17]. We used C implementation version 2.0 of SIPeS from `http://gmdd.shgmo.org/Computational-Biology/ChIP-Seq/download/SIPeS`. In our computational experiments and data analysis, we both used its default parameters and also considered alternative values for the parameters that define the range of the dynamic baseline to construct the signal map. SIPeS constructs signal map by piling up the aligned paired-end reads. [17] observed that SIPeS was able to attain high resolution for binding event identification when used with a wide range of dynamic baseline. Therefore, we investigated the performance of SIPeS when the DNA fragment pileups corresponding to two binding events are above (Fig. S15a, b) and within the range of dynamic baseline (Fig. S15c) in our computational experiments as described in the main manuscript. We observed that tuning the range of the dynamic baseline is far from trivial. Furthermore, a global value across the whole genome is not likely to perform well. There are also no guidelines or objective ways of configuring such a range.

Figure S15a shows that SIPeS has low sensitivity when two binding events are closely spaced. In this case, the value of the DNA fragment pileups between these two binding events did not belong to the range of dynamic baseline and, as a result, SIPeS identified the whole region as a single peak. Hence, although two binding events reside within this peak, SIPeS reported only a single *summit*. In contrast, Figure S15b shows that, on average, SIPeS identified more than 10 binding events when the distance between two binding events is larger than average library size. For these settings, there were some regions with low DNA fragment pileup within the range of the dynamic baseline between the two binding events. As a result, SIPeS essentially identified all local maxima as binding events and this resulted in low positive predicted value of SIPeS.

When the values of the DNA fragment pileups corresponding to the binding events are within the range of dynamic baseline, SIPeS is able to identify the two binding events (Figure S15c). However, SIPeS also identified all other local maxima as binding events and exhibited significant loss of positive predicted value. We also note that the SIPeS predictions corresponding to true binding events could not be distinguished from others, using the other summary statistics such as p-value or maximum fragment pileup value provided by SIPeS.

Finally, we evaluated SIPeS predictions for the 8 experimentally validated regions

of σ^{70} PET ChIP-Seq data. As discussed in the manuscript, these regions harbor a total of 14 experimentally validated σ^{70} binding sites. Figure S15d illustrates that dPeak attains significantly higher resolution compared to SIPeS in these regions (p-value of the paired t-test between dPeak and SIPeS < 0.01). Furthermore, although these regions harbor at most two validated σ^{70} binding sites, SIPeS predicted 2 to 18 binding sites. In summary, SIPeS does not sufficiently leverage PET ChIP-Seq data to provide high resolution for studying protein-DNA interactions. Furthermore, it is also highly sensitive to background noise in ChIP-Seq data and requires parameter tuning. We also note that the analysis of high depth PET ChIP-Seq data, such as that of σ^{70}, using SIPeS requires using wider ranges of dynamic baseline. This, in turn, increases the computation time significantly. Overall, it seems computationally prohibitive to implement a genome-wide analysis of such data using SIPeS, i.e., analysis of σ^{70} required more than 72 hours on a standard 64 bit machine with Intel Xeon 3.0GHz processor.

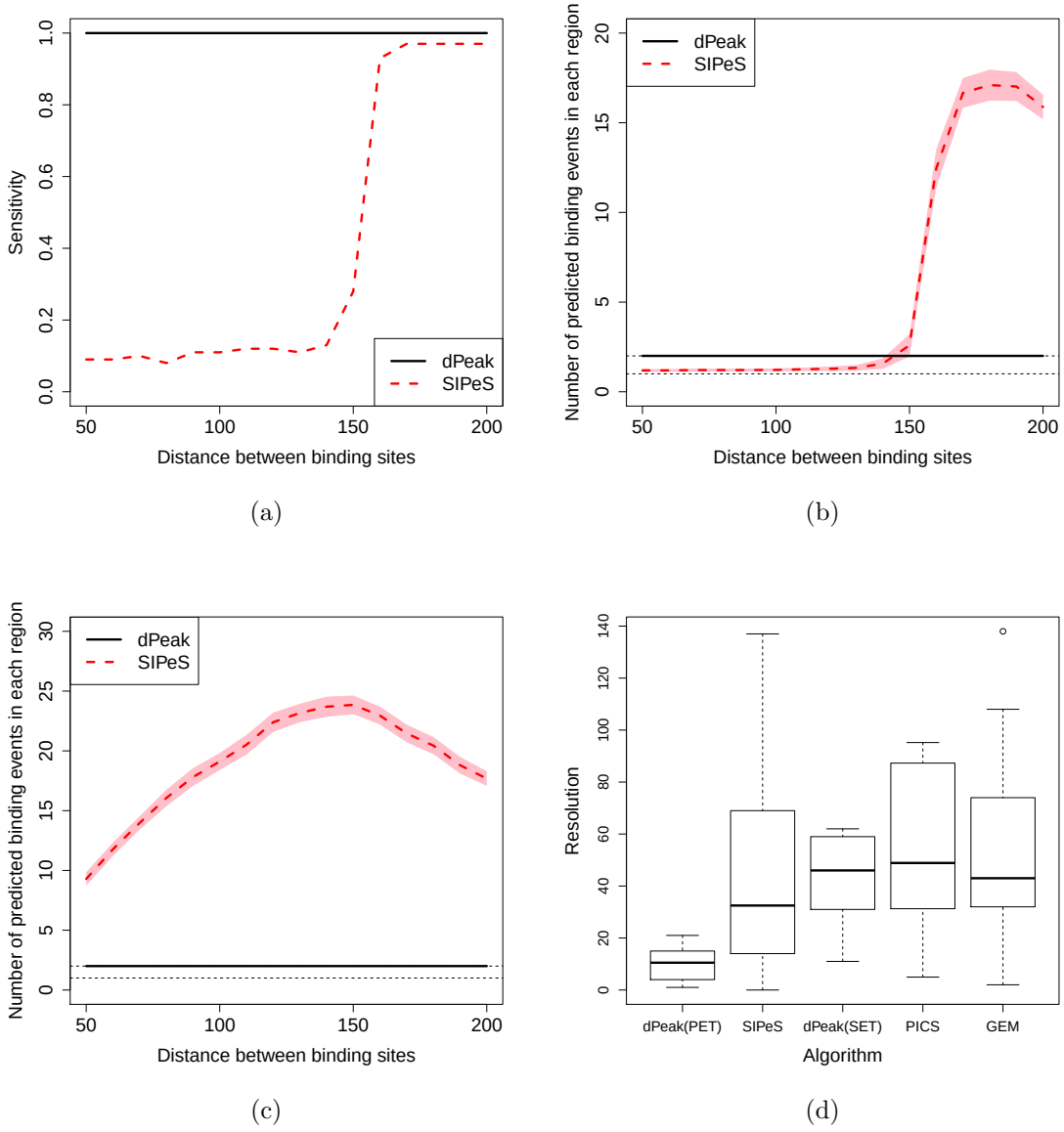

Figure S15: Evaluation of the SIPeS algorithm on PET ChIP-Seq data. Sensitivity and positive predicted value comparisons of SIPeS and dPeak for the computational experiments of PET ChIP-Seq data when DNA fragment pileup corresponding to two binding events is (a, b) and is not (c) within the range of dynamic baseline of SIPeS. (d) Resolutions of predictions for σ^{70} PET and quasi-SET ChIP-Seq data using experimentally validated binding sites as a gold standard.

17 Application of dPeak to a GATA1 SET ChIP-Seq Peak

In this section, we discuss an application of dPeak in eukaryotic genomes using the GATA1 SET ChIP-Seq data from [18]. This dataset has 106,381,508 reads and measures GATA1 occupancy in G1E-ER4 cells after estradiol treatment. GATA1 is known to bind to short consensus sequence WGATAR (W = A or T, R = A or G) [19]. A typical GATA1 ChIP-Seq peak on average harbors 2.32 WGATAR sites in this dataset. Being able to identify which of these are occupied is important for refining consensus sequences and deriving functional roles of about 7 million WGATAR sites in the mouse genome. Figure S16 displays coverage plot of the GATA switch site of the GATA2 locus (-2.8 kb). This region contains four WGATAR motifs separated by 20*bp* to 109*bp*. dPeak predicts that GATA1 factor binds to the second consensus site.

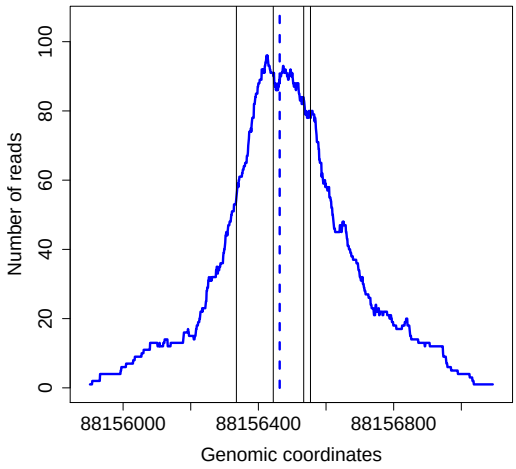

Figure S16: Coverage plot and dPeak prediction for the GATA switch site of the GATA2 locus. Blue curve and blue dotted vertical line indicate the GATA1 SET ChIP-Seq data from [18] and the prediction using the dPeak algorithm, respectively. Black solid vertical lines indicate positions of the GATA1 consensus sequences, [AT]GATA[AG].

18 Evaluations on Human SET ChIP-Seq Data

We evaluated the performance of dPeak on human SET ChIP-Seq data that GPS and PICS were optimized for. We considered GABPA SET ChIP-Seq data in GM12878 cell line from the ENCODE database. We identified 2,469 candidate regions using MOSAiCS (FDR = 1e-20) and these candidate regions were explicitly provided to the GPS and GEM algorithms as candidate regions. Candidate regions for PICS were identified using the function `segmentReads()` in the `PICS` R package (default parameters). Default tuning parameters were used during model fitting for all the methods.

In the case of a sequence-specific factor with well-conserved motif such as the GABPA factor, we observed that dPeak prediction can be further improved in a straightforward way by incorporating sequence information. Specifically, after identifying initial dPeak predictions, we identified a *de novo* motif using MEME [20] and detected positions of these consensus sequences using FIMO [21]. Then, we updated the dPeak predictions if the GABPA consensus sequences were found within the $50bp$ window around initial dPeak predictions. We call these dPeak predictions that integrate sequence information as 'dPeak2'.

Figure S17 shows resolution comparison on the GABPA-GM12878 dataset. The resolution is defined as the absolute distance to the nearest predicted consensus site, where the prediction utilizes the independent position weight matrix from JASPAR [22]. The results indicate that dPeak performs comparable to GPS (median resolution = 18 bp and 19 bp for dPeak and GPS, respectively) and they both significantly outperform PICS (median resolution = 30 bp). Moreover, dPeak2 performs comparable to GEM and identifies the GABPA binding sites with high accuracy.

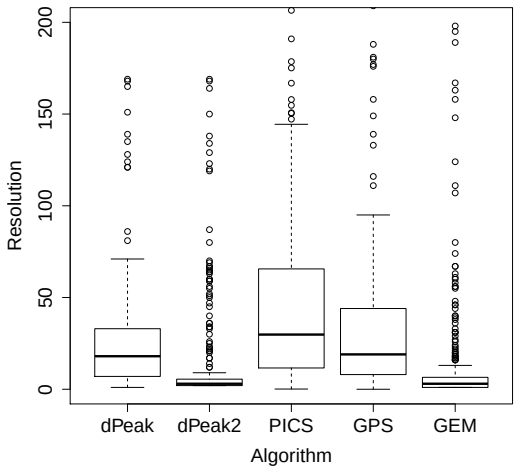

Figure S17: Resolutions of predictions for ENCODE GABPA-GM12878 SET ChIP-Seq Data, using positions of GABPA consensus sequences as identified by the JASPAR position weight matrix scan as a gold standard.

19 Comparison of dPeak using SET ChIP-Seq with ChIP-exo

ChIP-exo [23] is a modified ChIP-Seq protocol that aims to experimentally identify binding sites at high resolution by employing exonuclease. ChIP-exo protocol is more laborious compared to ChIP-Seq and there are not many available ChIP-exo datasets yet. Despite these limitations, we investigated how ChIP-Seq analysis with dPeak compared to ChIP-exo analysis for identifying binding sites in high resolution. We evaluated ChIP-exo data measuring binding of CTCF factor in human HeLa-S3 cell line (downloaded from SRA with accession number SRA044886). Although [23] did not generate ChIP-Seq data in parallel to this ChIP-exo data, we were able to utilize SET ChIP-Seq data for CTCF factor in human HeLa-S3 cell line from the ENCODE project (Crawford Lab, Duke University). For both ChIP-exo and ChIP-Seq data, all the available replicates were combined.

In order to evaluate the performance of ChIP-exo data, we utilized predictions provided in [23]. These predictions were generated using a combination of an automated tool for analyzing ChIP-exo data in a strand-specific manner and a set of manually curated rules by inspection of the data. For comparison, we also generated predictions of dPeak, GPS, and GEM for CTCF ChIP-exo and SET ChIP-Seq data. We did not consider PICS because it is not tailored for the ChIP-exo data analysis. We also generated dPeak2 predictions by utilizing sequence information using the same procedure as described in Section 18. We utilizes the CTCF position weight matrix from JASPAR [22], as a gold standard.

Figure S18 shows proportion of CTCF consensus sequences identifed at a given spatial resolution of each method at given spatial resolution. The results indicate that dPeak and dPeak2 using ChIP-exo data shows spatial resolution comparable to or better than predictions of [23], GPS, and GEM, which implies that dPeak can readily be utilized in ChIP-exo data analysis. It also shows that predictions using CTCF ChIP-Seq data provide significantly higher spatial resolution compared to predictions using CTCF ChIP-exo data.

References

[1] Zhang Y, Liu T, Meyer CA, Eeckhoute J, Johnson DS, et al. (2008) Model-based analysis of ChIP-Seq (MACS). Genome Biol 9: R137.

[2] Kuan PF, Chung D, Pan G, Thomson JA, Stewart R, et al. (2011) A statistical framework for the analysis of ChIP-Seq data. J Am Stat Assoc 106: 891–903.

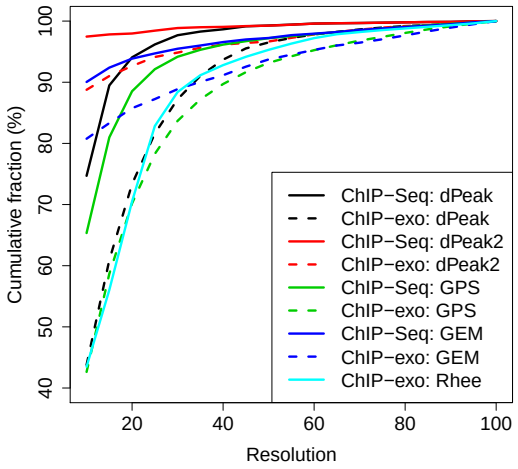

Figure S18: Comparison of cumulative fraction as a function of spatial resoltion, for ChIP-exo data and SET ChIP-seq data of CTCF factor in human HeLa-S3 cell line. Cumulative fraction is defined as proportion of CTCF consensus sequences identifed by each method at a given spatial resolution.

[3] Dempster AP, Laird NM, Rubin DB (1977) Maximum likelihood from incomplete data via the EM algorithm. J R Stat Soc, Series B 39: 1–38.

[4] Meng XL, Rubin DB (1993) Maximum likelihood estimation via the ECM algorithm: a general framework. Biometrika 80: 267–278.

[5] McLachlan G, Peel D (2000) Finite Mixture Models. Wiley, New York.

[6] McLachlan G, Krishnan T (2008) The EM Algorithm and Extensions. Wiley, New York.

[7] Celeux G, Diebolt J (1985) The SEM algorithm: a probabilistic teacher algorithm derived from the EM algorithm for the mixture problem. Comput Stat Q 2: 73–82.

[8] Crawford S (1994) An application of the Laplace method to finite mixture distributions. J Am Stat Assoc 89: 259–267.

[9] Schwarz G (1978) Estimating the dimension of a model. Ann Stat 6: 461–464.

[10] Fraley C, Raftery A (1998) How many clusters? Which clustering method? Answers via model-based cluster analysis. Comput J 41: 578–588.

[11] Fraley C, Raftery AE (2002) Model-based clustering, discriminant analysis, and density estimation. J Am Stat Assoc 97: 611–631.

[12] Gama-Castro S, Salgado H, Peralta-Gil M, Santos-Zavaleta A, Muniz-Rascado L, et al. (2011) RegulonDB version 7.0: transcriptional regulation of *Escherichia coli* K-12 integrated within genetic sensory response units (Gensor Units). Nucleic Acids Res 39: D98–D105.

[13] Zhang X, Robertson G, Krzywinski M, Ning K, Droit A, et al. (2011) PICS: probabilistic inference for ChIP-seq. Biometrics 67: 151–163.

[14] Guo Y, Papachristoudis G, Altshuler RC, Gerber GK, Jaakkola TS, et al. (2010) Discovering homotypic binding events at high spatial resolution. Bioinformatics 26: 3028–3034.

[15] Guo Y, Mahony S, Gifford DK (2012) High resolution genome wide binding event finding and motif discovery reveals transcription factor spatial binding constraints. PLoS Comput Biol 8: e1002638.

[16] Homann OR, Johnson AD (2010) MochiView: versatile software for genome browsing and DNA motif analysis. BMC Biol 8: 49.

[17] Wang C, Xu J, Zhang D, Wilson Z, Zhang D (2010) An effective approach for identification of *in vivo* protein-DNA binding sites from paired-end ChIP-Seq data. BMC Bioinformatics 11: 81.

[18] Wu W, Cheng Y, Keller CA, Ernst J, Kumar SA, et al. (2011) Dynamics of the epigenetic landscape during erythroid differentiation after GATA1 restoration. Genome Res 21: 1659–1671.

[19] Bresnick EH, Lee HY, Fujiwara T, Johnson KD, Keleş S (2010) GATA switches as developmental drivers. J Biol Chem 285: 31087-31093.

[20] Bailey TL, Elkan C (1994) Fitting a mixture model by expectation maximization to discover motifs in biopolymers. ISMB94 : 28–36.

[21] Grant CE, Bailey TL, Noble WS (2011) FIMO: Scanning for occurrences of a given motif. Bioinformatics 27: 1017-1018.

[22] Bryne JC, Valen E, Tang MH, Marstrand T, Winther O, et al. (2008) JASPAR, the open access database of transcription factor-binding profiles: new content and tools in the 2008 update. Nucleic Acids Res 36: D102–D106.

[23] Rhee HS, Pugh BF (2011) Comprehensive genome-wide protein-DNA interactions detected at single-nucleotide resolution. Cell 147: 1408-1419.

a

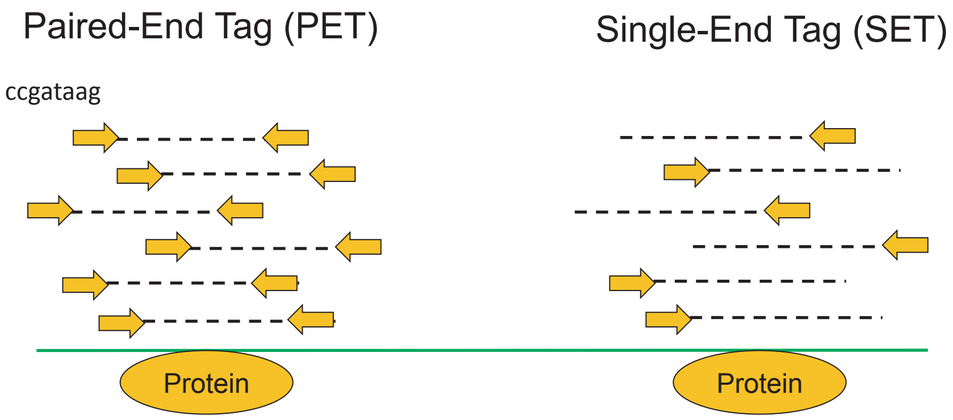

b

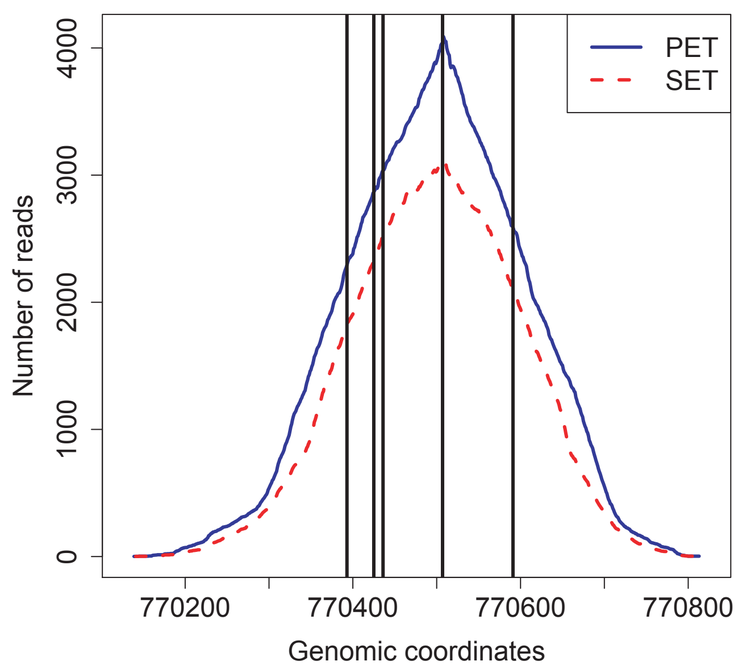

c

1. Identify candidate regions in low resolution, using the genome-wide analysis.

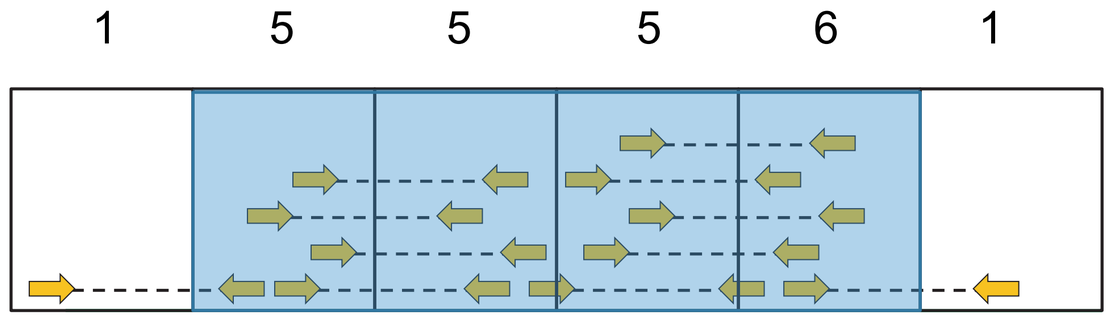

2. For each candidate region, extract reads corresponding to the region.

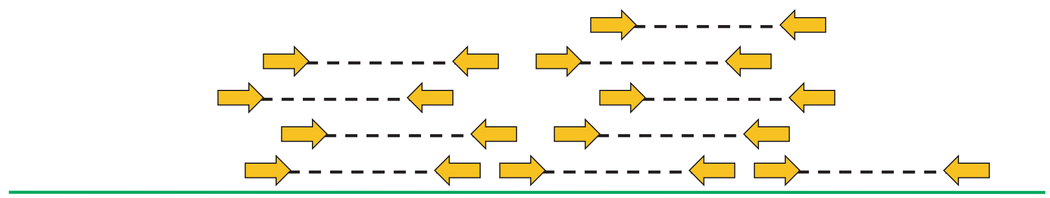

3. For each candidate region, identify binding sites in high resolution, using the dPeak model.

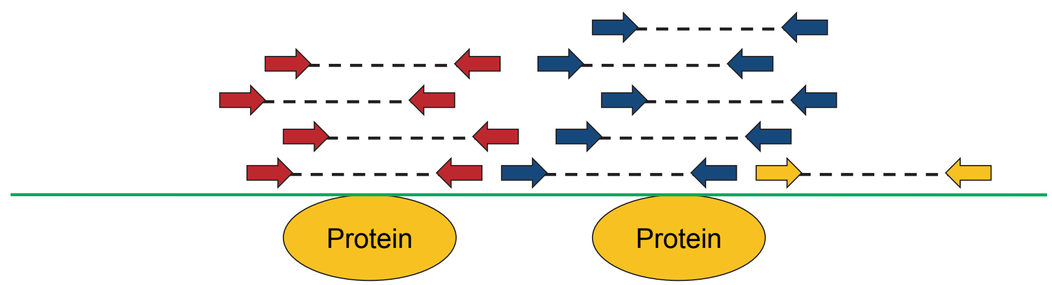

A

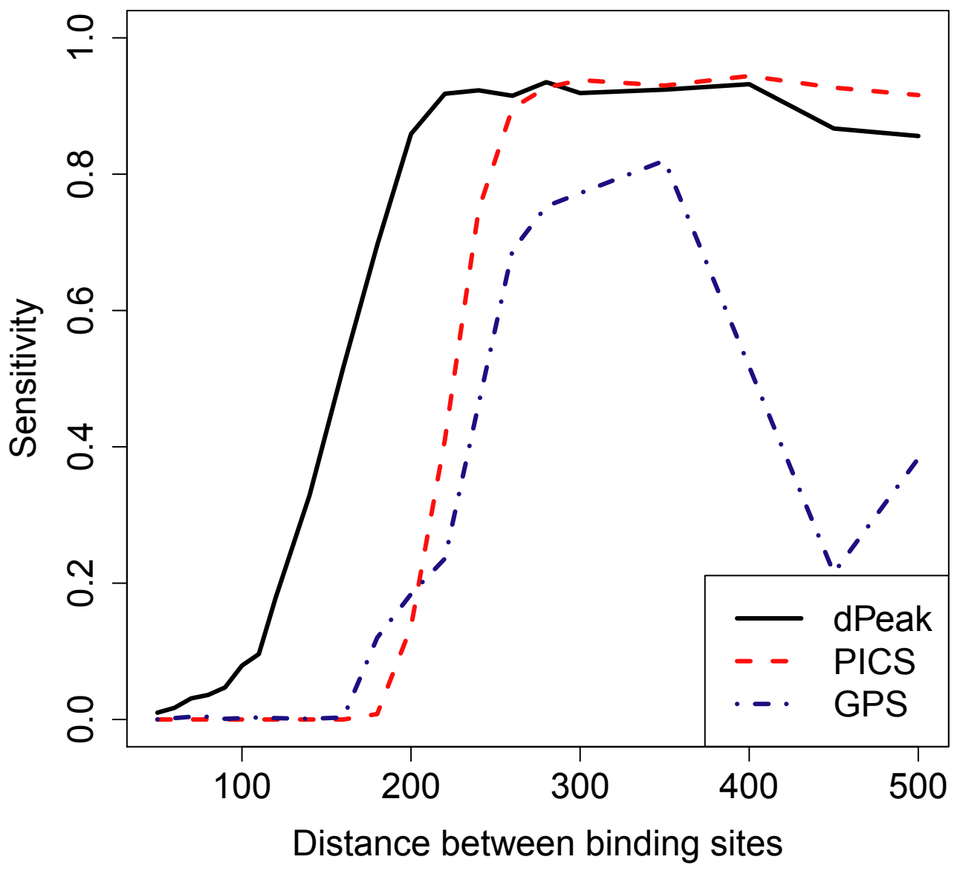
Sensitivity
0.0
0.2
0.4
0.6
0.8
1.0
100
200
300
400
500
Distance between binding sites
dPeak
PICS
GPS

B

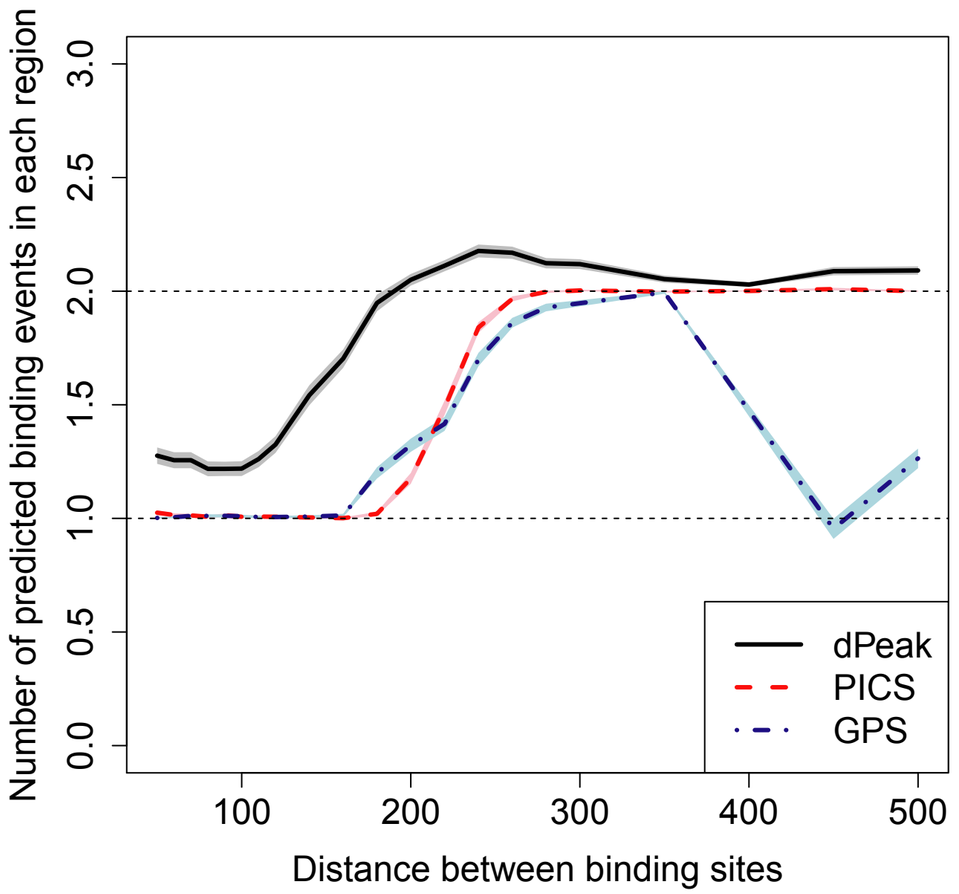
Number of predicted binding events in each region
0.0
0.5
1.0
1.5
2.0
2.5
3.0
100
200
300
400
500
Distance between binding sites
dPeak
PICS
GPS

C

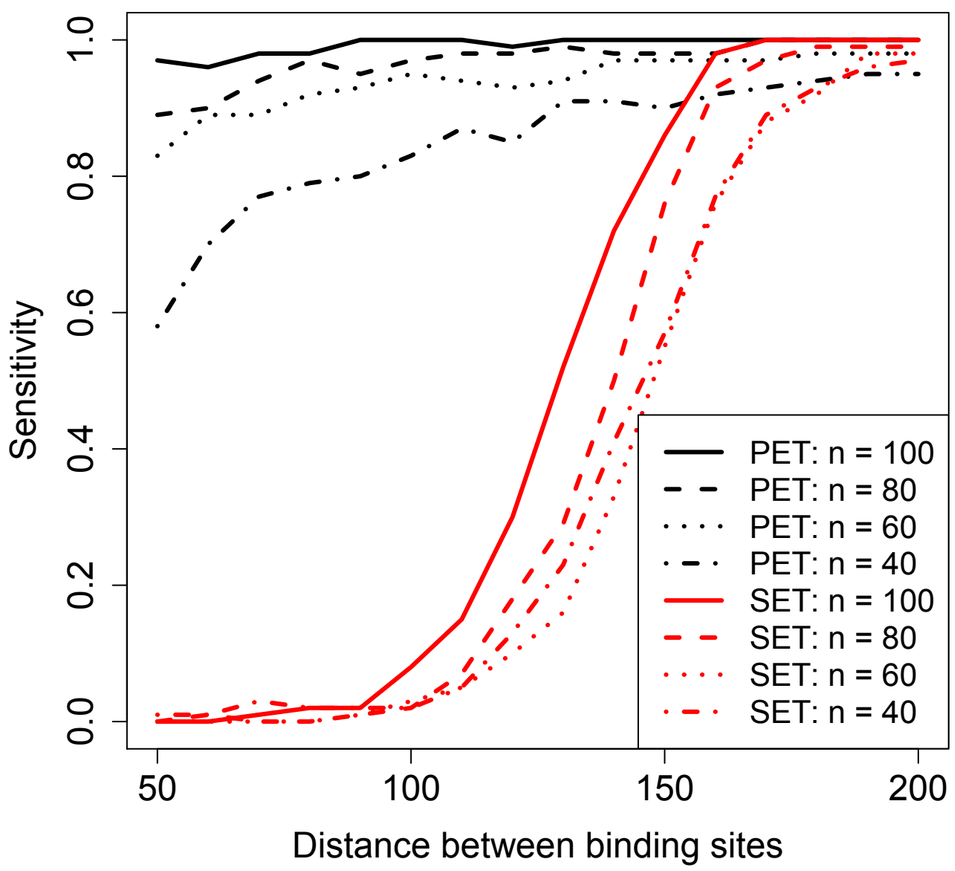
Sensitivity
0.0
0.2
0.4
0.6
0.8
1.0
50
100
150
200
Distance between binding sites
PET: n = 100
PET: n = 80
PET: n = 60
PET: n = 40
SET: n = 100
SET: n = 80
SET: n = 60
SET: n = 40

D

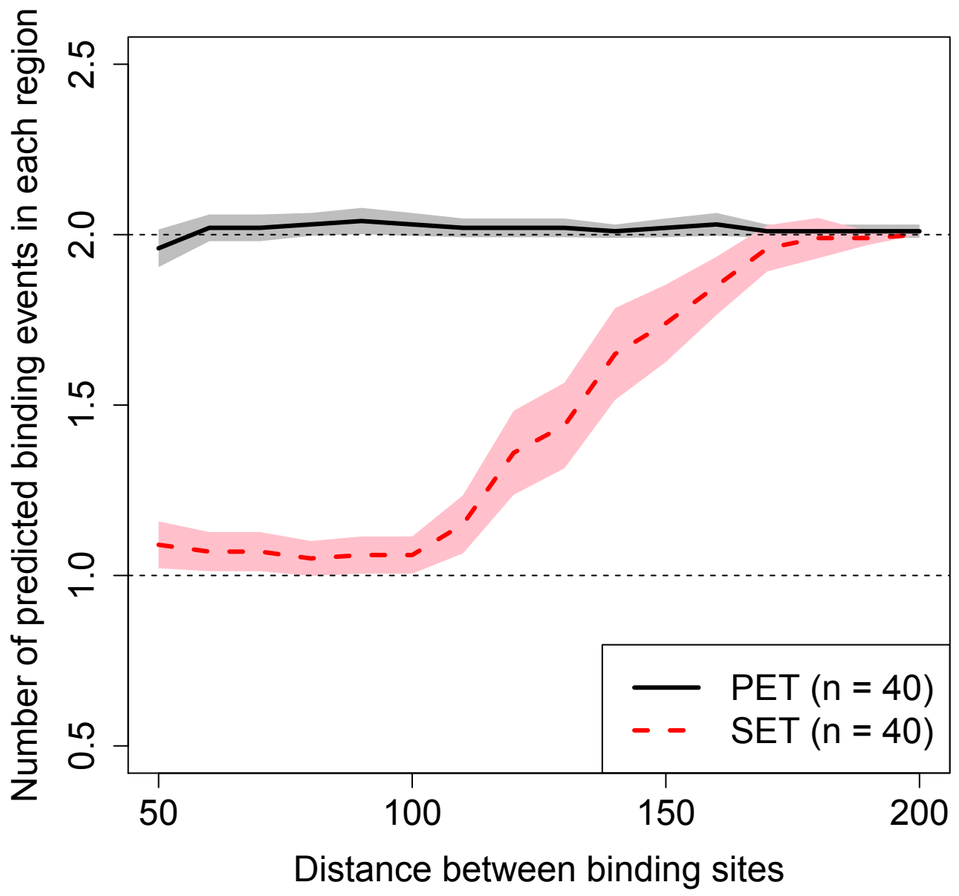
Number of predicted binding events in each region
0.5
1.0
1.5
2.0
2.5
50
100
150
200
Distance between binding sites
PET (n = 40)
SET (n = 40)

A

Invasion

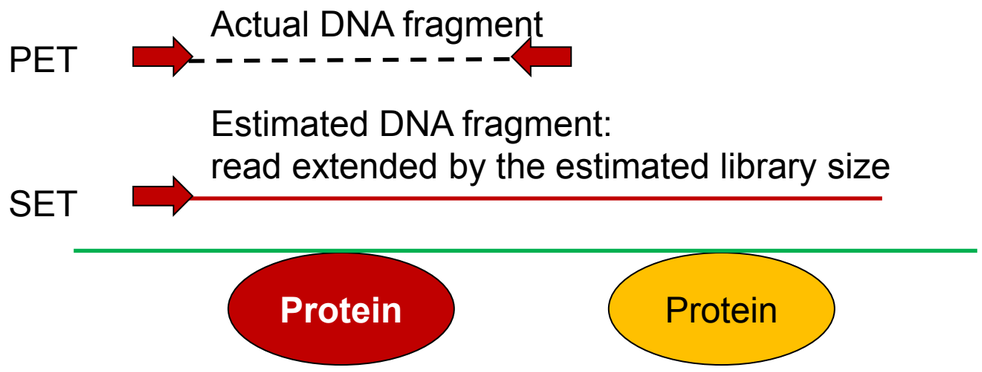

Truncation

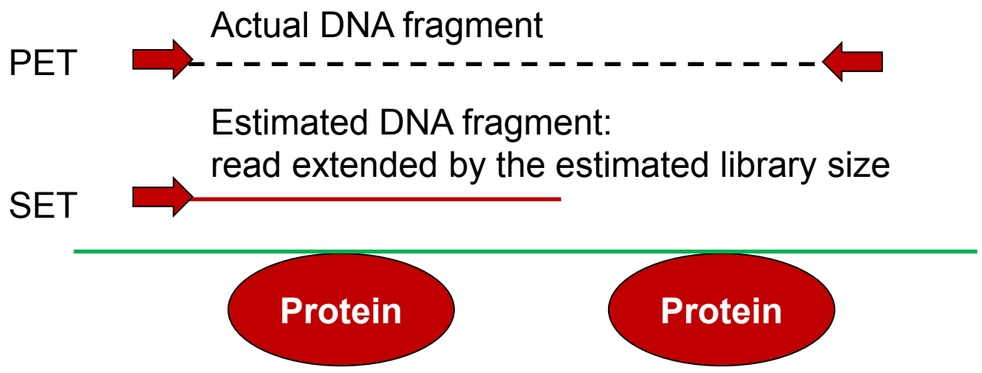

B

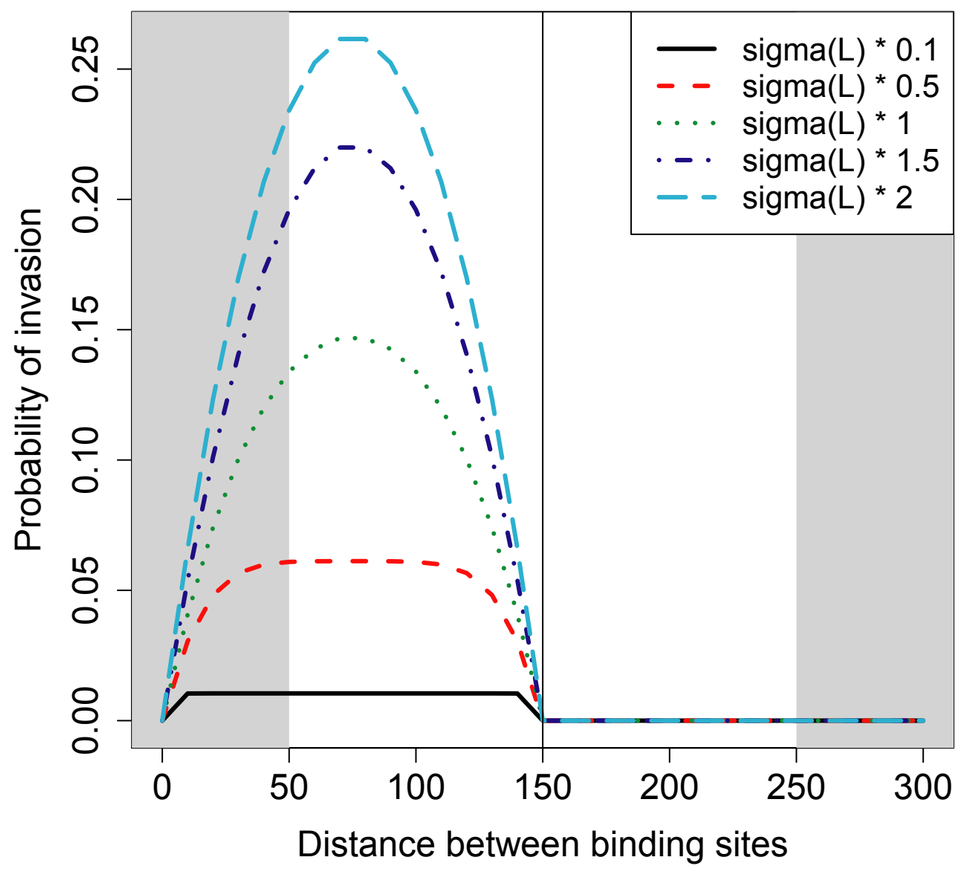

C

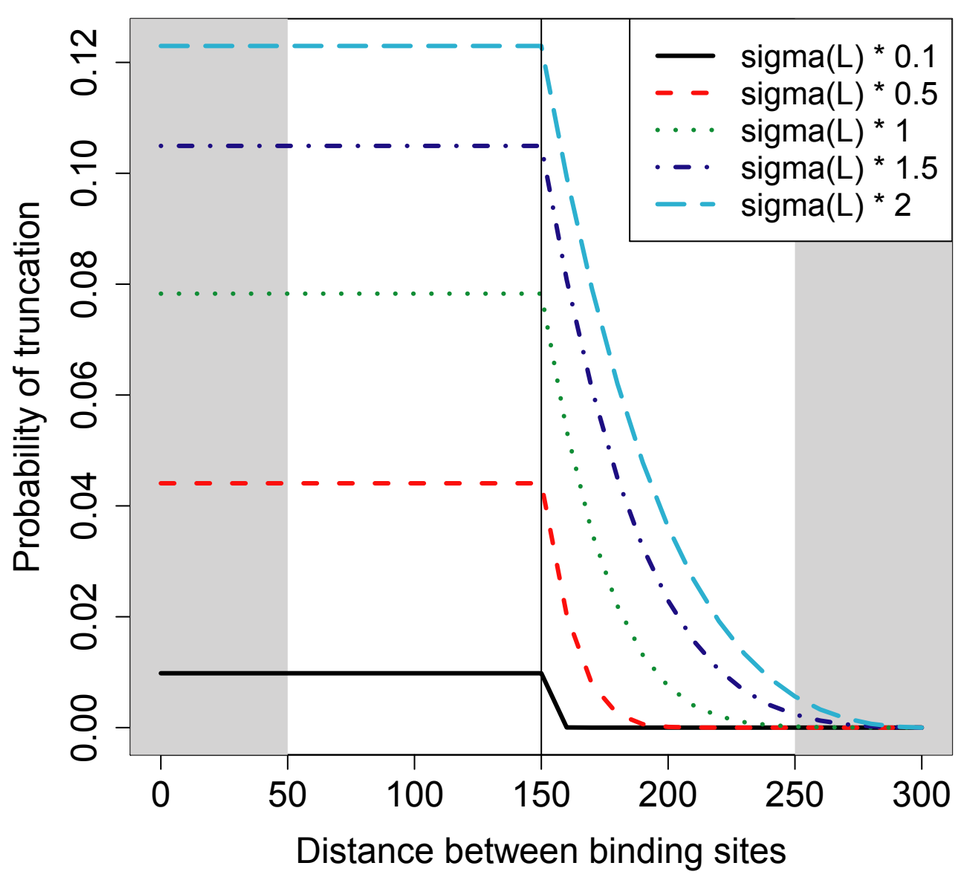

A

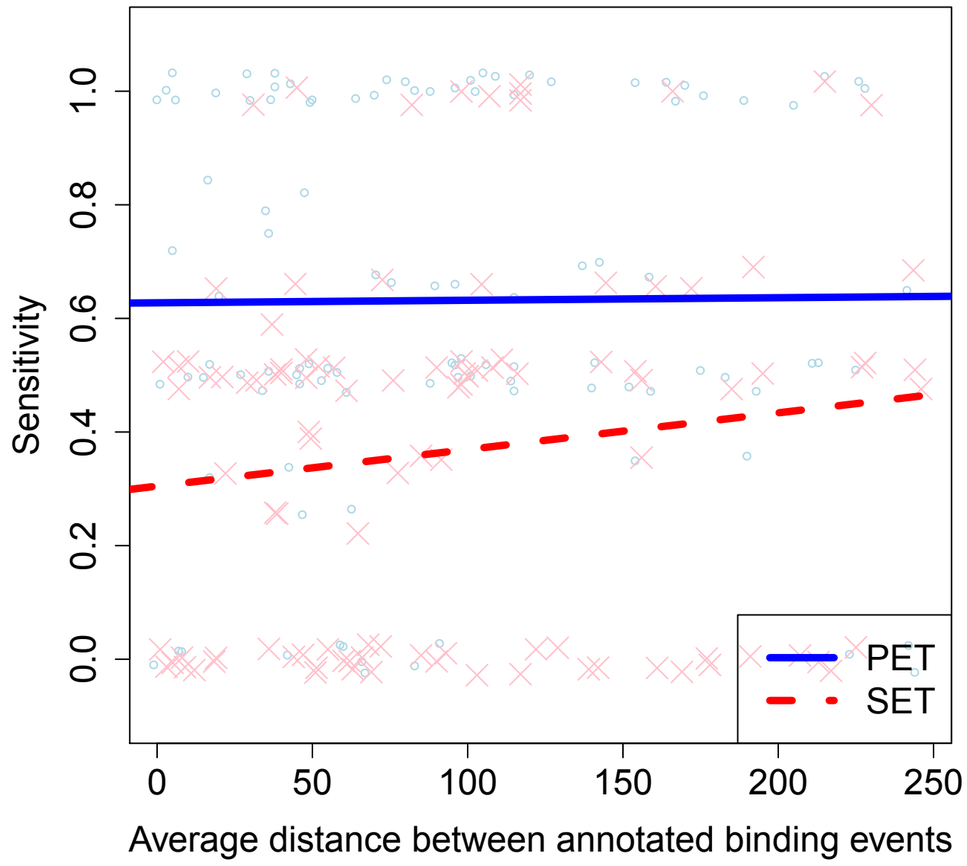
Sensitivity
0.0
0.2
0.4
0.6
0.8
1.0
0
50
100
150
200
250
Average distance between annotated binding events
PET
SET

B

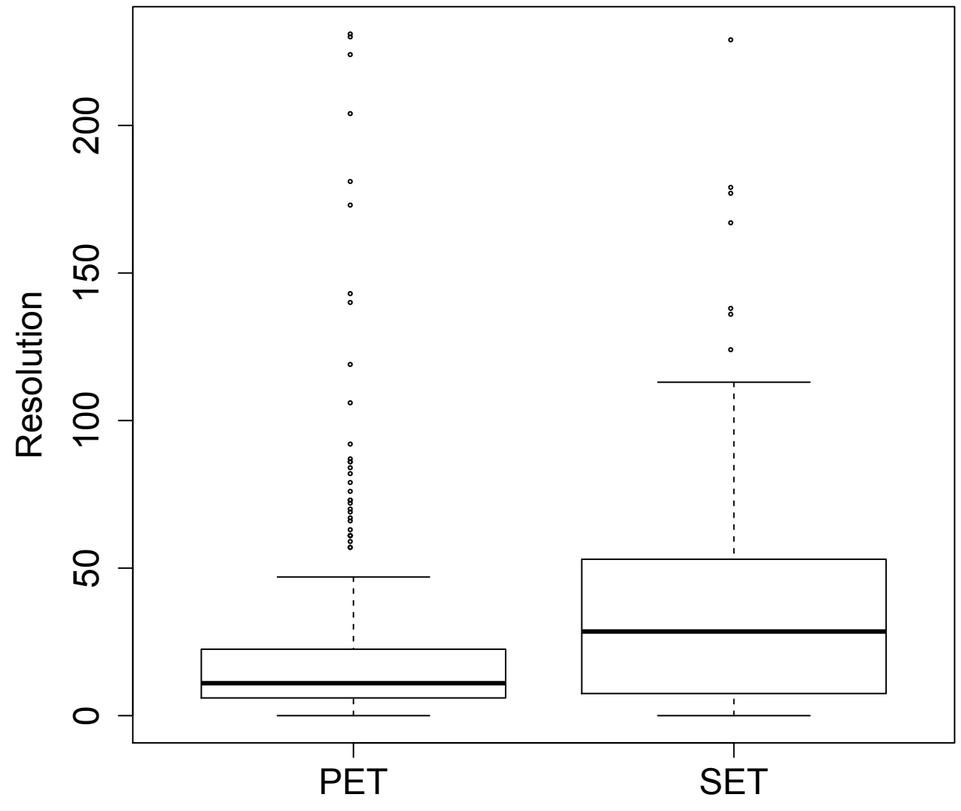
Resolution
0
50
100
150
200
PET
SET

C

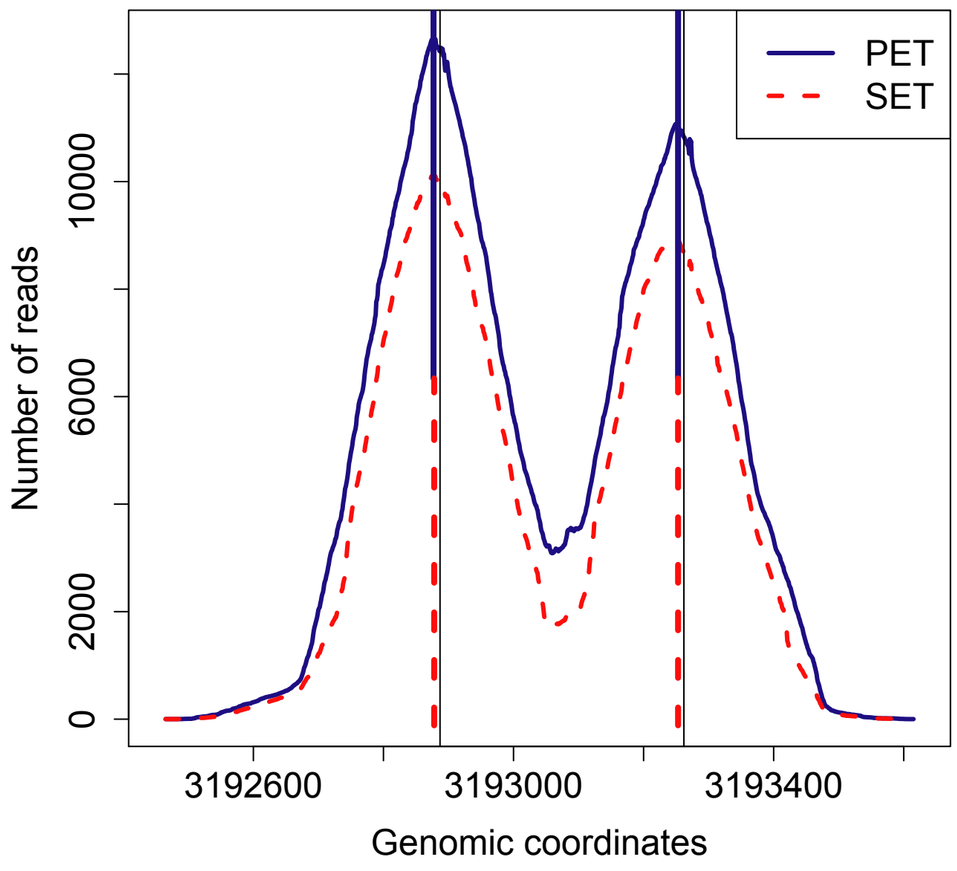
Number of reads
0
2000
6000
10000
3192600
3193000
3193400
Genomic coordinates
PET
SET

D

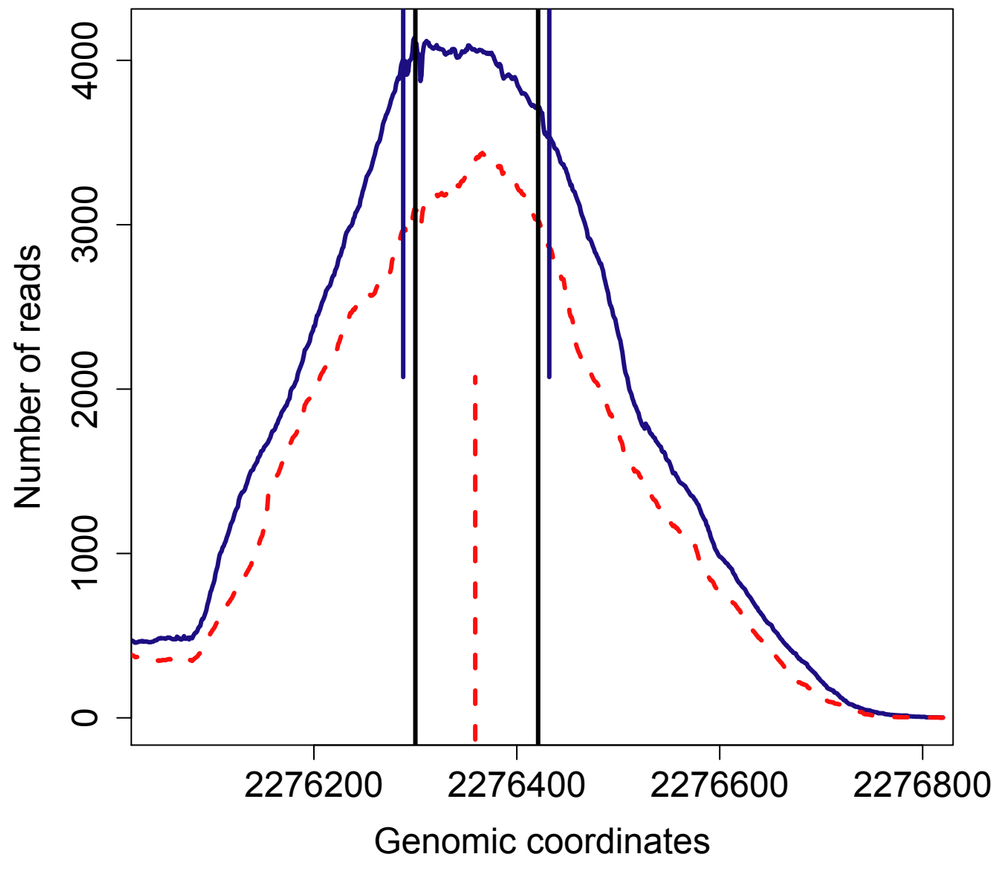
Number of reads
0
1000
2000
3000
4000
2276200
2276400
2276600
2276800
Genomic coordinates

A

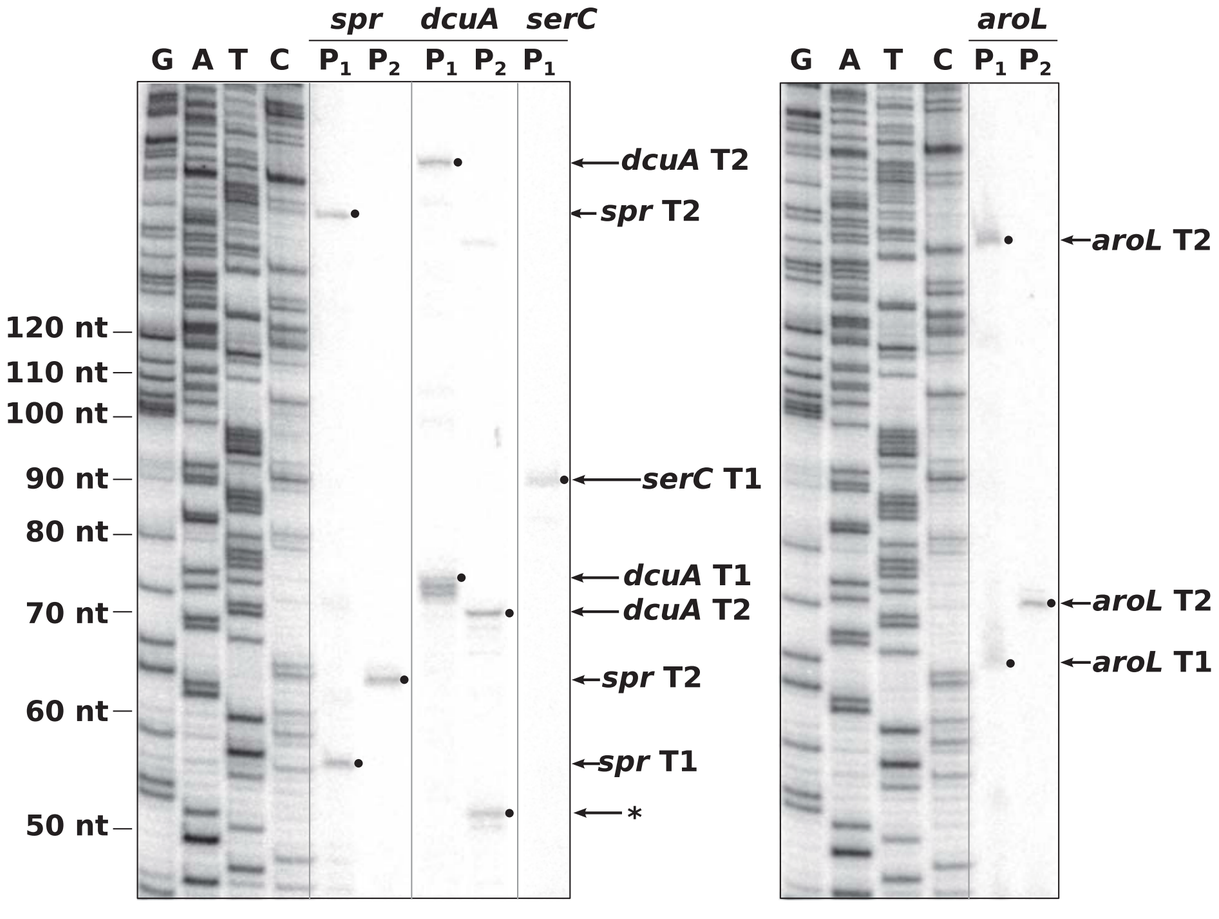
spr
dcuA
serC
G A T C
P1 P2 P1 P2 P1
dcuA T2
spr T2
120 nt
110 nt
100 nt
90 nt
80 nt
serC T1
dcuA T1
70 nt
dcuA T2
spr T2
60 nt
spr T1
50 nt
*

aroL
G A T C
P1 P2
aroL T2
aroL T2
aroL T1

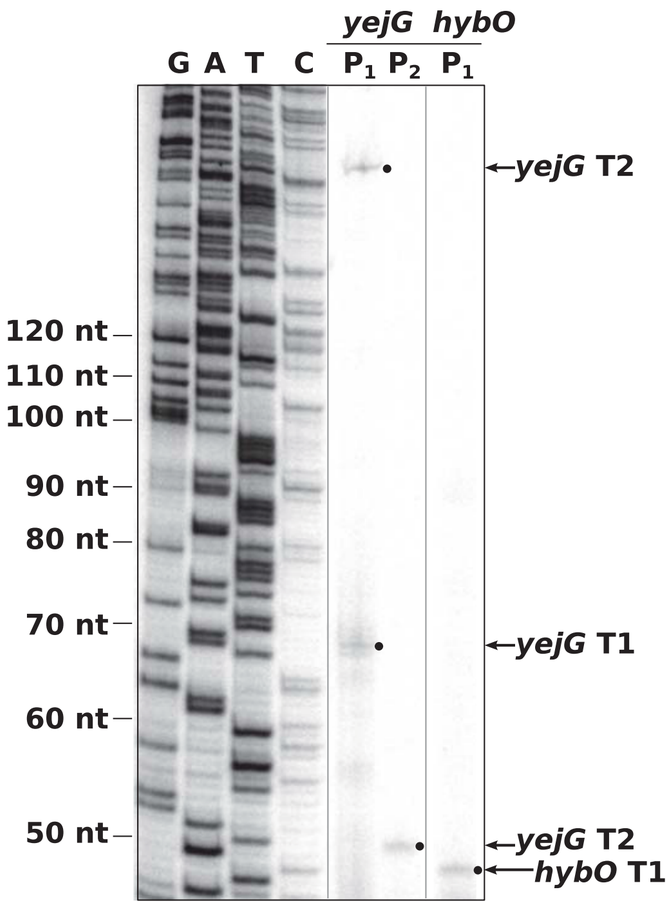
yejG hybO
G A T C
P1 P2 P1
yejG T2
120 nt
110 nt
100 nt
90 nt
80 nt
70 nt
yejG T1
60 nt
50 nt
yejG T2
hybO T1

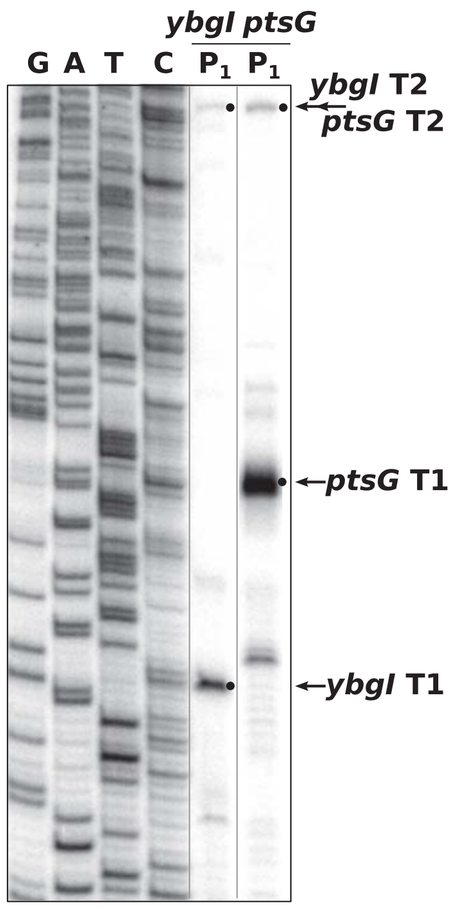
ybgI ptsG
G A T C
P1 P1
ybgI T2
ptsG T2
ptsG T1
ybgI T1

B

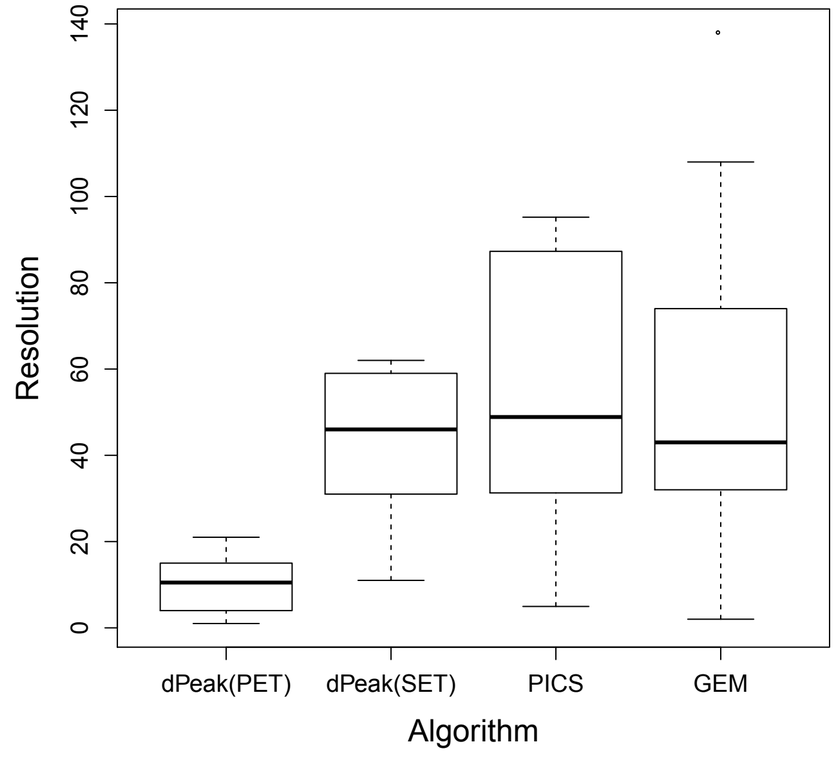
Resolution
0
20
40
60
80
100
120
140
dPeak(PET)
dPeak(SET)
PICS
GEM
Algorithm

C

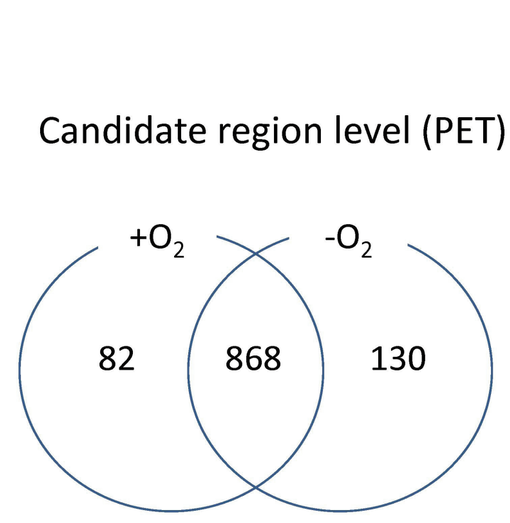
Candidate region level (PET)
+O2
-O2
82
868
130

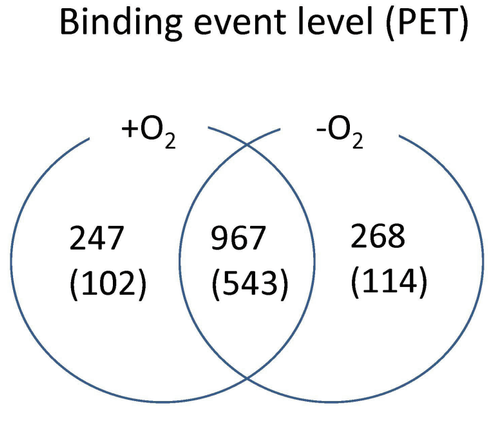
Binding event level (PET)
+O2
-O2
247
(102)
967
(543)
268
(114)